Supplementary Materials for

Pathway Engineering of Multicomponent Self-Assembly in $M_{12}L_{24}$ Nanospheres with Pseudorotaxanes

Authors: T. Bouwens,[1†] E. O. Bobylev,[1] D. A. Poole III,[1‡] S. Mathew,[1] J. N. H. Reek[1]*

Affiliations:

[1] van 't Hoff Institute for Molecular Sciences, Universiteit van Amsterdam, Science Park 904, 1098 XH Amsterdam, The Netherlands.

[†] Yusuf Hamied Department of Chemistry, University of Cambridge, Lensfield Road, Cambridge, UK

[‡] De Boelelaan 1108, O|2 building, 1081 HZ Amsterdam, The Netherlands

*Corresponding author. Email: j.n.h.reek@uva.nl

* Email: j.n.h.reek@uva.nl

Contents

S1. Material and methods

S1.1. General

All reagents and solvents were obtained from Sigma-Aldrich, Fluorochem and VWR and were used without any purification. Compound **1** and **ring** were obtained following literature procedure.[1] Ligand $\mathbf{L^{MeO}}$ was prepared following literature procedure by Yang and coworkers.[2] MeCN and THF were dried in a solvent purification system. Column chromatography was performed using silica gel (SiliCycle, SiliaFlash P60, 40–63 μm, 230–400 mesh) while fractions were analyzed using TLC (TLC silica gel 60 F254 from Merck KGaA) visualized with 254/350 nm light. Products were analyzed using MS, NMR and IR. ^{1}H NMR and ^{13}C NMR spectra were recorded on a Bruker AV300, AV400 and AV500 spectrometer and are reported in ppm using a solvent residual signal as internal standard (7.26 ppm for $CDCl_3$ and 1.94 ppm for CD_3CN). DOSY ^{1}H NMR spectral data was acquired with temperature and magnetic gradient calibration prior to the measurements, and the temperature was kept at 298 K during the measurements unless indicated otherwise. Exact mass of the compounds was obtained on an AccuTOF GC v 4g, JMS-T100GCV Mass spectrometer (JEOL, Japan) equipped with an FD Emitter, Carbotec or Linden (Germany), FD 13 μm. Current rate 51.2 mA min^{-1} over 1.2 min machine using field desorption (FD) as ionization method. UV–vis measurements were performed on a single beam Hewlett Packard 8453 spectrometer in a quartz cuvette using MeCN as background. IR spectra were recorded on a Bruker Alpha FTIR machine.

S1.2. Synthesis

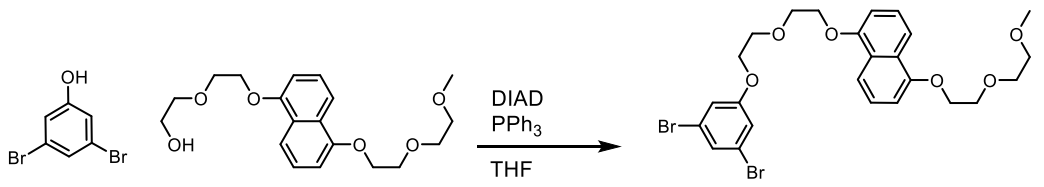

3,5-Dibromophenol **1** **2**

<u>*Compound 2:*</u> Compound **1** (1.5 g, 4.3 mmol, 1 equiv.), 3,5-dibromophenol (1.19 g, mmol, 1.1 equiv.) and PPh_3 (1.41 g, 5.4 mmol, 1.25 equiv.) were dissolved in dry THF (120 mL). To this DIAD (1.086 g, 1.057 mL, 5.4 mmol, 1.25 equiv.) was added and the mixture was stirred over night at room temperature. TLC confirmed presence of a new species. The THF was removed and the crude mixture was purified by column chromatography (DCM:EtOAc, 3:2, v/v). After removal of the organic solvents by rotary evaporation a white sticky solid was obtained (2.65 g, 63%). The final product contained diisopropyl hydrazine-1,2-dicarboxylate (~30 wt% based on NMR) (byproduct of Mitsunobu coupling using DIAD), and was used without further purification for synthesis of $\mathbf{L}^{\mathbf{DNP}}$. ^{1}H NMR (300 MHz, CD_3CN) δ 7.79 (t, J = 8.8 Hz, 2H), 7.45 – 7.31 (m, 2H), 7.30 (t, J = 1.5 Hz, 1H), 7.09 (d, J = 1.5 Hz, 2H), 6.99 – 6.89 (m, 2H), 4.33 – 4.21 (m, 4H), 4.19 – 4.09 (m, 2H), 4.02 – 3.85 (m, 6H), 3.76 – 3.56 (m, 3H), 3.52 (dd, J = 5.6, 3.7 Hz, 2H), 3.31 (d, J = 1.0 Hz, 3H). ^{13}C NMR (75 MHz, CD_3CN) δ 160.33, 154.32, 154.29, 126.57, 126.07, 125.39, 125.35, 122.82, 114.12, 114.06, 105.96, 105.91, 70.35, 69.49, 69.36, 69.20, 69.03, 68.43, 68.06, 57.93. HRMS (FD–MS) (*m/z*): $[M]^+$ $C_{25}H_{28}Br_2O_6$ calculated: 582.02526; found:582.0268. FT–IR (neat): 3301, 2980, 2934, 2876, 1710, 1509, 1375, 1225, 1178, 1106, 1042, 930, 857.

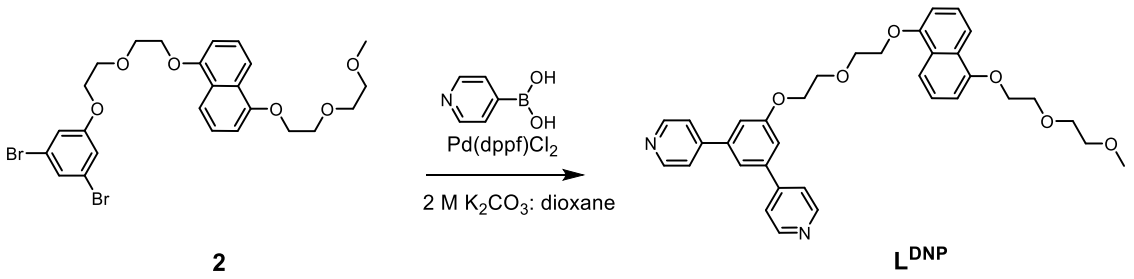

2 **L^{DNP}**

Compound ***L^{DNP}***: To a mixture of compound **2** (298 mg, 0.511 mmol, 1 equiv.) and 4-pyridinylboronic acid (251.24 mg, 2.04 mmol, 4 equiv.) in dioxane (56 mL), $K_2CO_{3(aq)}$ (2 M, 7 mL) in water was added. The mixture was degassed with N_2 for one hour before adding $Pd(dppf)Cl_2$ (56.1 mg 0.077 mmol, 15mol%) and the mixture was stirred at 80°C overnight. The dioxane was removed by rotary evaporation, after which water (200 mL) was added. The organics were extracted by washing the water with EtOAc (3 × 200 mL). The organic layers were combined and dried (Na_2SO_4), filtered and EtOAc was evaporated. The crude mixture was purified by column chromatography (DCM:MeOH, 19:1). After removal of the organic solvents by rotary evaporation a white powder was obtained (169 mg, 57%). mp: 101.2°C, ^{1}H NMR (500 MHz, CD_3CN) δ 8.61 (dd, 2H), 7.78 (d, J = 8.5 Hz, 1H), 7.64 (dd, 2H), 7.60 (t, 1H), 7.40 – 7.24 (m, 2H), 6.91 (dd, J = 28.8, 7.7 Hz, 1H), 4.36 – 4.27 (m, 2H), 4.26 – 4.20 (m, 1H), 4.05 – 3.96 (m, 2H), 3.93 – 3.87 (m, 1H), 3.72 – 3.66 (m, 1H), 3.54 – 3.48 (m, 1H), 3.30 (s, 1H). ^{13}C NMR (75 MHz, CD_3CN) δ 161.09, 155.26, 151.23, 148.18, 141.27, 127.51, 126.34, 122.69, 119.23, 115.07, 115.03, 114.82, 106.86, 106.81, 72.65, 71.33, 70.61, 70.52, 70.31, 69.07, 68.99, 58.91, 1.32. HRMS (FD–MS) (*m/z*): $[M]^+C_{35}H_{36}N_2O_6$ calculated: 580.2573; found 580.2549. FT–IR (neat): 3059, 3028, 2925, 2876, 1591, 1549, 1508, 1412, 1346, 1265, 1204, 1133, 1078, 969, 816, 775.

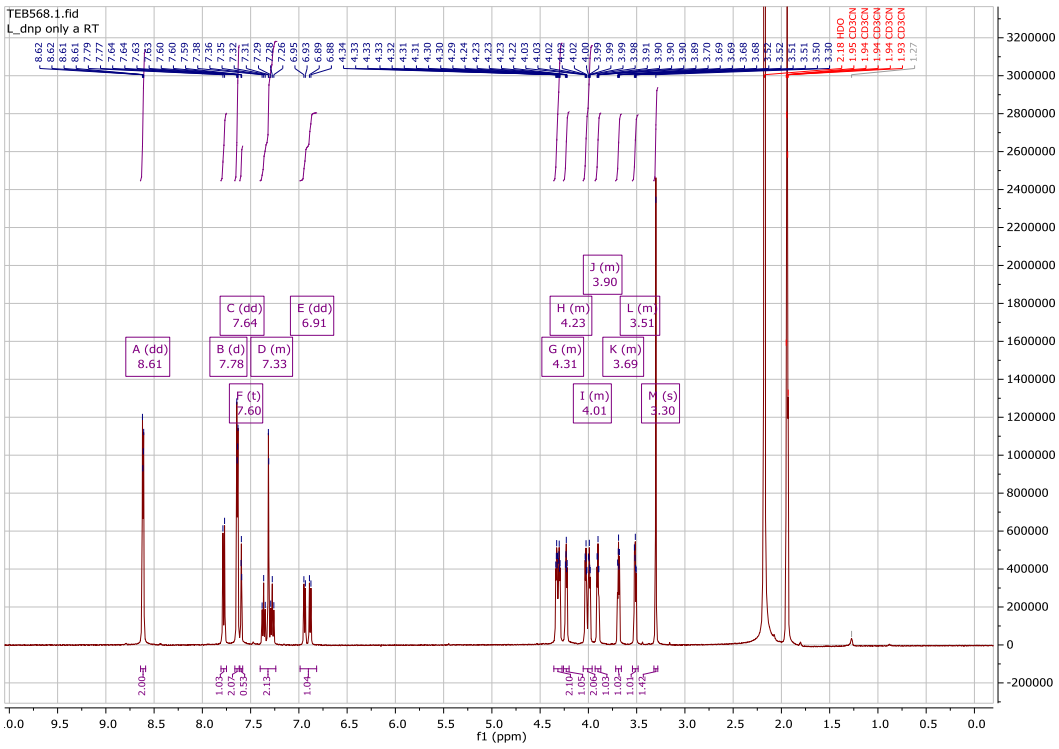

Figure 1. ^{1}H NMR spectrum of the final product $\mathbf{L}^{\mathbf{DNP}}$ (500 MHz, 298 K) in CD_3CN.

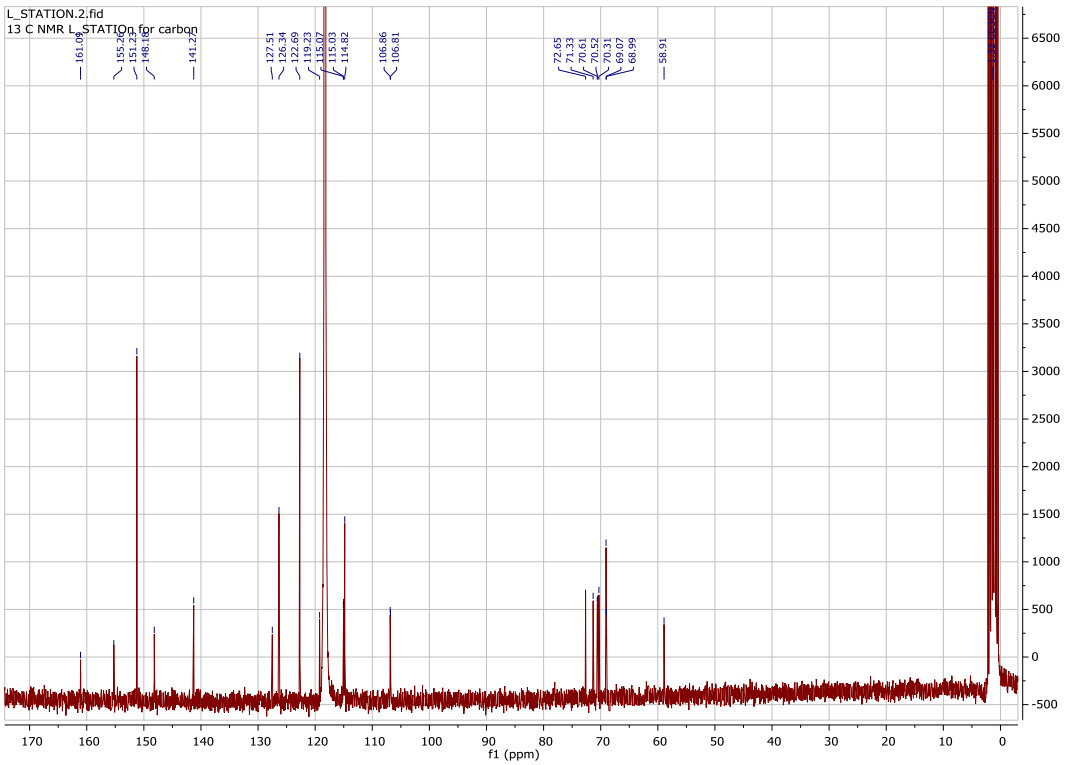

Figure 2. ^{13}C NMR spectrum of the final product $\mathbf{L}^{\mathbf{DNP}}$ (500 MHz, 298 K) in CD_3CN.

S1.3. Procedure NMR studies at 25°C

*Pathway 2 (with **ring**):* The ligand $\mathbf{L^{DNP}}$ (5.61 mg, 9.66 µmol, 1.93 equiv.) and **ring** (10.6 mg, 9.66 µmol, 1.93 equiv.) were dissolved in CD_3CN (0.9 mL). To this solution, $Pd(MeCN)_4(BF_4)_2$ (5 µmol, 1 equiv., 100 µL of a 50 mM CD_3CN solution) was added. To obtain the nanosphere, the sample was stirred overnight at room temperature (25°C).

*Pathway 1 (without **ring**):* The ligand $\mathbf{L^{DNP}}$ (5.61 mg, 9.66 µmol, 1.93 equiv.) was dissolved in CD_3CN (0.9 mL). To this, $Pd(MeCN)_4(BF_4)_2$ (5 µmol, 1 equiv., 100 µL of a 50 mM CD_3CN solution) was added. To obtain the nanosphere, the sample was stirred overnight at room temperature (25°C). After this, **ring** (10.6 mg, 9.66 µmol, 1.93 equiv.) can be added to obtain the pseudorotaxane nanosphere.

[(ring) ⊂Pd(L^{DNP})$_{24}$] *PF_6 nanosphere for mass analysis:* The ligand $\mathbf{L^{DNP}}$ (5.61 mg, 9.66 µmol, 1.93 equiv.) and **ring** (10.6 mg, 9.66 µmol, 1.93 equiv.) are dissolved in CD_3CN (0.9 mL). To this, $Pd(MeCN)_4(PF_6)_2$ (5 µmol, 1 equiv., 100 µL of a 50 mM CD_3CN solution) was added. To obtain the nanosphere, the sample was stirred overnight at room temperature (25°C).

S1.4. Procedure kinetic NMR studies

*Pathway 1 (without **ring**):* The ligand $\mathbf{L^{DNP}}$ (5.61 mg, 9.66 µmol, 1.93 equiv.) was dissolved in CD_3CN (0.9 mL). From this mixture 0.54 mL was added to an NMR tube and the first ^1H NMR is recorded at the correct temperature. After this $Pd(MeCN)_4(BF_4)_2$ (3 µmol, 1equiv., 60 µL of a 50 mM CD_3CN solution) is added and the solution is mixed by a vortex. The kinetic NMR sequence starts directly after mixing. Kinetics were measured overnight, recording NMR at 10–15 minute intervals. After the experiment, a ^1H NMR and ^1H DOSY NMR spectra are recorded at room temperature. This is repeated 2 days after the experiment to determine the end point and ensure all Pd–L polymer has converted into nanosphere.

*Pathway 2 (with **ring**):* The ligand $\mathbf{L^{DNP}}$ (5.61 mg, 9.66 µmol, 1.93 equiv.) and **ring** (10.6 mg, 9.66 µmol, 1.93 equiv.) was dissolved in CD_3CN (0.9 mL). From this mixture 0.54 mL was added to an NMR tube and the first ^1H NMR is recorded at the correct temperature. After this $Pd(MeCN)_4(BF_4)_2$ (3 µmol, 1equiv., 60 µL of a 50 mM CD_3CN solution) is added and the solution is mixed by a vortex. The kinetic NMR sequence starts directly after mixing. Kinetics were measured overnight, recording NMR at 10–15 minute intervals. After the experiment, a ^1H NMR and ^1H DOSY NMR spectra are recorded at room temperature. This is repeated 2 days after the experiment to determine the end point and ensure all Pd–L polymer has converted into nanosphere.

Pathway switch 14°C: The ligand $\mathbf{L^{DNP}}$ (5.61 mg, 9.66 µmol, 1.93 equiv.) is dissolved in CD_3CN (0.9 mL). From this solution 0.54 mL is added to an NMR tube and the first ^1H NMR is recorded at 14°C. After this a stock solution of $Pd(MeCN)_4(BF_4)_2$ (3 µmol, 1equiv., 60 µL of a 50 mM CD_3CN solution) is added and the solution is mixed by a vortex. The kinetic NMR sequence starts

directly after mixing. Kinetics are measured every 10 minutes for 30 minutes. Then **ring** is added while the sample is kept at 0°C so no reaction can take place. Switching kinetics are measured overnight and NMR is recorded every 10 minutes. After the experiment, a ^{1}H NMR and a DOSY is recorded at room temperature. This is repeated 2 days after the experiment to determine the end point and ensure all Pd–L polymer has converted into nanosphere.

Nanosphere formation with ***L^{DNP}*** *and* ***[MV(PF$_6$)$_2$]****:* The ligand $\mathbf{L^{DNP}}$ (5.61 mg, 9.66 µmol, 1.93 equiv.) and **[MV(PF$_6$)$_2$]** (10.6 mg, 19.32 µmol, 3.86 equiv.) are dissolved in CD_3CN (0.9 mL). From this solution 0.54 mL is added to an NMR tube and the first ^{1}H NMR is recorded at 25°C. A stock solution of $Pd(MeCN)_4(BF_4)_2$ (3 µmol, 1equiv., 60 µL of a 50 mM CD_3CN solution) is added and the solution is homogenized by vortex mixing. Directly after addition a precipitate was formed. ^{1}H NMR solely shows the signals belonging to $\mathbf{MV^{2+}}$.

Nanosphere formation with ***L^{MeO}*** *and* ***ring****:* The ligand $\mathbf{L^{MeO}}$ (5.61 mg, 9.66 µmol, 1.93 equiv.) and **ring** (10.6 mg, 9.66 µmol, 1.93 equiv.) are dissolved in CD_3CN (0.9 mL). From this solution 0.54 mL is added to an NMR tube and the first ^{1}H NMR is recorded at 25°C. After this $Pd(MeCN)_4(BF_4)_2$ (3 µmol, 1equiv., 60 µL of a 50 mM CD_3CN solution) is added and the solution is homogenized by vortex mixing. Kinetics are measured overnight and ^{1}H NMR and DOSY is recorded every 10 minutes. After the experiment, a ^{1}H NMR and a DOSY is recorded at 25°C.

S1.5. ESI–MS studies

*Pathway 2 (with **ring**):* The ligand $\mathbf{L}^{\mathbf{DNP}}$ (5.61 mg, 9.66 µmol, 1.93 equiv.) and **ring** (10.6 mg, 9.66 µmol, 1.93 equiv.) are dissolved in CD_3CN (0.9 mL). To this a stock solution of $Pd(MeCN)_4(BF_4)_2$ (5 µmol, 1 equiv., 100 µL of a 50 mM CD_3CN solution) was added the solution is homogenized by vortex mixing. The kinetic MS sequence starts directly after mixing and is performed at room temperature. At each time point, 50 uL were taken out of the solution, diluted with 50 uL MeCN and the corresponding mass spectra were measured. The final spectra (final intensities) were measured with a sample of nanosphere with **ring** prepared by the conventional synthesis route (Pathway 2) which was also diluted to 50% using MeCN. After the experiment, ^{1}H NMR and DOSY ^{1}H NMR spectra are recorded at room temperature to confirm the end point.

*Pathway 1 (without **ring**):* The ligand $\mathbf{L}^{\mathbf{DNP}}$ (5.61 mg, 9.66 µmol, 1.93 equiv.) is dissolved in CD_3CN (0.9 mL). To this a stock solution of $Pd(MeCN)_4(BF_4)_2$ (5 µmol, 1 equiv., 100 µL of a 50 mM CD_3CN solution) was added the solution is homogenized by vortex mixing. The kinetic MS sequence starts directly after mixing and is performed at room temperature. At each time point, 50 µL were taken out of the solution and the corresponding MS spectra was measured. The final spectra (final intensities) were measured with a sample of nanosphere B prepared by the conventional synthesis route. After the experiment, ^{1}H NMR and DOSY ^{1}H NMR spectra are recorded at room temperature to confirm the end point.

Pathway switch: The ligand $\mathbf{L}^{\mathbf{DNP}}$ (5.61 mg, 9.66 µmol, 1.93 equiv.) is dissolved in CD_3CN (0.9 mL). To this a stock solution of $Pd(MeCN)_4(BF_4)_2$ (5 µmol, 1 equiv., 100 µL of a 50 mM CD_3CN solution) was added the solution is homogenized by vortex mixing. The kinetic MS sequence starts

directly after mixing and is performed at room temperature. Kinetics are measured every 10 minutes for 30 minutes. At each time point, 50 uL were taken out of the solution and the corresponding MS spectra was measured Then **ring** is added and directly a sample is measured. At each time point, 50 uL were taken out of the solution, diluted with 50 uL MeCN and the corresponding MS spectra was measured. The final spectra (final intensities) were measured with a sample of sphere A prepared by the conventional synthesis route which was also diluted to 50% using MeCN. After the experiment, a ^{1}H NMR and a DOSY ^{1}H NMR spectra are recorded at room temperature. This is repeated 2 days after the experiment to make sure all Pd–L polymer has converted into nanosphere to determine the end point.

S1.6. Binding studies

***DNP** recognition site and the **ring**:* In order to determine K_{ass} of the $\mathbf{L}^{\mathbf{DNP}}$ site and the **ring**, a solution of **ring** was kept at a constant concentration (500 μM) and was titrated with an increasing concentration of **ring** (20 mM) inside a cuvette of 10 mm path length. After every addition of $\mathbf{L}^{\mathbf{DNP}}$ the UV–vis absorption spectrum was recorded to check the extinction at 525 nm. The data was fitted to a 1:1 host–guest model using a Matlab script.[3]

*Nanosphere and **ring**:* To study the interaction between **ring** and the nanosphere, a solution of **ring** was kept at a constant concentration (38.6 μM) and was titrated with an increasing concentration of **ring** (20 mM) inside a cuvette of 10 mm path length. After every addition of $\mathbf{L}^{\mathbf{DNP}}$ the UV–vis absorption spectrum was recorded to check the extinction at 525 nm.

Molar absorptivity nanosphere: To determine the extinction coefficient of the charge transfer complex between $\mathbf{L}^{\mathbf{DNP}}$ and **ring**, a 575 μM [$\mathbf{L}^{\mathbf{DNP}}$:**ring]** solution was prepared in MeCN from 1.15 mM stock solutions of **ring** and 9.3 mM $\mathbf{L}^{\mathbf{DNP}}$ stock solution. These solutions were mixed 1:1 and a purple color emerged. The absorption was measured against MeCN as background on a 2 mm pathlength quartz cuvette. Next a nanosphere solution (4.6 mM $\mathbf{L}^{\mathbf{DNP}}$-nanosphere) containing 4.6 mM **ring** ($\mathbf{L}^{\mathbf{DNP}}$-nanosphere: **ring** = 1:1) was prepared from a 9.66 mM pseudorotaxane stock solution. The absorption was measured against MeCN as background on a 2 mm path length quartz cuvette.

S2. Characterization and binding studies

S2.1. Characterization of the $Pd_{12}(L^{DNP})_{24}$ nanosphere and its components

The two formation processes of interest are the formation of ***$Pd_{12}(L^{DNP})_{24}$*** nanosphere in presence of **ring** (Pathway 2) and in absence of **ring** (Pathway 1), respectively yielding the pseudorotaxane-decorated $Pd_{12}(\mathbf{L^{DNP}})_{24}(\mathbf{ring})_{8\pm5}$ nanosphere and the "bald" ***$Pd_{12}(L^{DNP})_{24}$*** nanosphere. Pseudorotaxane formation and nanosphere assembly are orthogonal self-assembly processes, consistent with observations in previous reports of similar cages and nanospheres featuring pseudorotaxanes.[4–7] The $Pd_{12}(\mathbf{L^{DNP}})_{24}(\mathbf{ring})_{8\pm5}$ pseudorotaxane nanosphere can be prepared in two different ways depending on when the **ring** is introduced: i) before addition of Pd^{2+} metal source (Figure 3a, Pathway 2) or ii) after formation of the $\mathbf{L^{DNP}}$ nanosphere (Figure 3a, Pathway 1), with either pathway yielding the same assembly.

Nanosphere formation is characterized by a downfield shift in the ligand pyridine signals (PyrA $\Delta\delta$ = 0.53 ppm and PyrB $\Delta\delta$ = 0.39 ppm) accompanied by a decrease in the diffusion constant (log*D* = -9.58) (Supplementary Figure 3a, b, Supplementary Table 1).

Pseudorotaxane formation between the electron deficient **ring** and the electron rich **DNP** moiety of $\mathbf{L^{DNP}}$ typically leads to a charge transfer (CT) band at visible wavelengths(λ_{max} = 525 nm), allowing for determination of the association constant K_{ass} between **ring** and the recognition site ($K_{ass} = 2.8 \times 10^3$ M^{-1}) of $\mathbf{L^{DNP}}$ upon fitting the titration data to a 1:1 model (Supplementary Figure 4a).[8] This strong interaction implies that a 1:1 **ring**:$\mathbf{L^{DNP}}$ complex is formed at the reaction conditions applied in this study. This is not the case for the interaction of **ring** to $\mathbf{L^{DNP}}$ nanosphere indicated by DOSY ^{1}H NMR (Supplementary Figure 3d) and lower absorption at 525 nm (Supplementary Figure 5c). ESI–MS shows that the pseudorotaxane nanosphere bears an average

of 8 **rings** (Supplementary Figure 27), i.e., approximately 30% of the 24 recognition sites on the outside of the nanosphere are occupied by **ring** (on average).

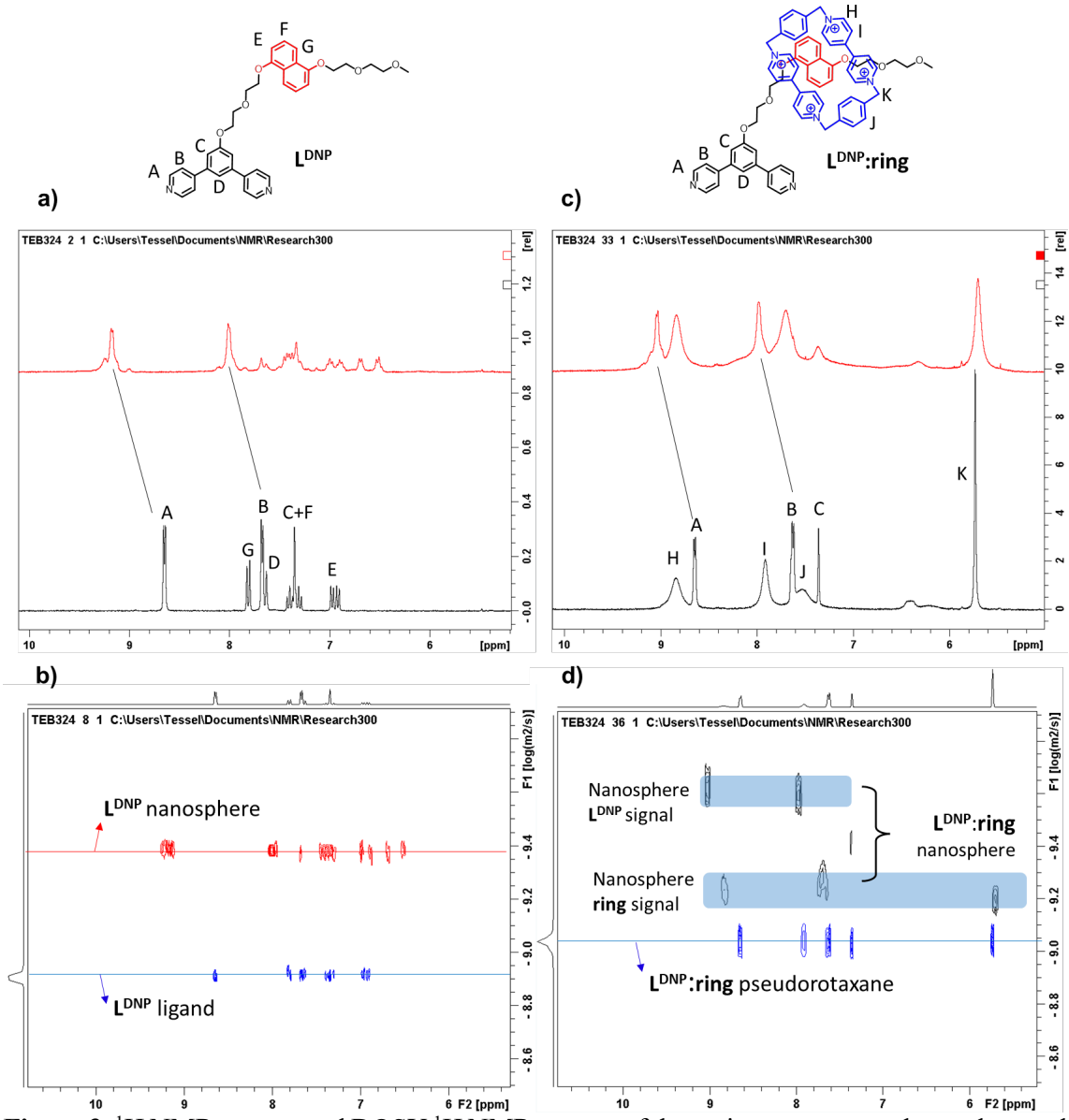

Figure 3. ^{1}H NMR spectra and DOSY ^{1}H NMR spectra of the main structures under study together with the molecular structures. a) $\mathbf{L^{DNP}}$ building block (black) shows a clear downfield shift in both the PyrA ($\Delta\delta$ = 0.53 ppm) and PyrB ($\Delta\delta$ = 0.39 ppm) signals when the $\mathbf{L^{DNP}}$ nanosphere is formed (red). b) Stacked DOSY ^{1}H NMR spectra of the ligand only (blue) and signals of the $\mathbf{L^{DNP}}$ nanosphere (red) at lower Log*D* value. c) Pseudorotaxane formation results in broadening of the ring signals and naphthalene signals. Upon pseudorotaxane nanosphere formation the pyridine signals shift downfield, but to a lesser extent than for $\mathbf{L^{DNP}}$ nanosphere formation: PyrA ($\Delta\delta$ = 0.37 ppm) and PyrB ($\Delta\delta$ = 0.36 ppm) d) DOSY ^{1}H NMR spectra of the $\mathbf{L^{DNP}}$**:ring** pseudorotaxane (blue) and signals of the pseudorotaxane $\mathbf{L^{DNP}}$**:ring** nanosphere (black) at lower Log*D* value. The blue spectrum consists of two parts. At smaller log*D* are the ring signals and at more negative log*D* values the signals for the ligand can be found. This means that there is exchange between ring bound to the nanosphere and free diffusing ring species.

Table 1. Diffusion properties of the nanospheres and its components used as a reference for the kinetic experiments measured with DOSY ^{1}H NMR. [a]The radius *r* can be determined by application of the Stokes–Einstein equation using Log*D* value (see Experimental Section 2.1.; (Equation 1.). [b]DOSY ^{1}H NMR shows two separate Log*D* values for the **$Pd_{12}(L^{DNP})_{24}(ring)_{8\pm5}$** pseudorotaxane–nanosphere belonging to the protons associated with the nanosphere and with **ring**.

Structure	L^{DNP}	**ring**	$L^{DNP}\subset$**ring**	$Pd_{12}(L^{DNP})_{24}$	$Pd_{12}(L^{DNP})_{24}$(**ring**)$_{8\pm5}$	$Pd_{12}(L^{MeO})_{24}$
Log*D* (Log(m^2 s^{-1})	-8.93	-9.03	-9.04	-9.58	-9.70 (-9.30)[b]	-9.46
r (nm)[a]	0.54	0.69	0.70	2.41	3.17	1.81

Stokes–Einstein equation

The Stokes–Einstein equation represented by Equation 1. is applied to estimate the radius of the nanosphere as is described previously.[9]

$$D = \frac{kT}{6\pi\eta r} \quad (1)$$

D = Diffusion coefficient (m^2 s^{-1})
k = Boltzman constant (1.38×10^{-23} N m K^{-1})
T = Temperature (298 K)
η = Viscosity of medium (CD_3CN at 298 K: 3.43×10^{-4} N m^{-2})
r = Radius (m)

S2.2. UV–vis characterization and binding data

Binding study **L^{DNP}** and **ring**

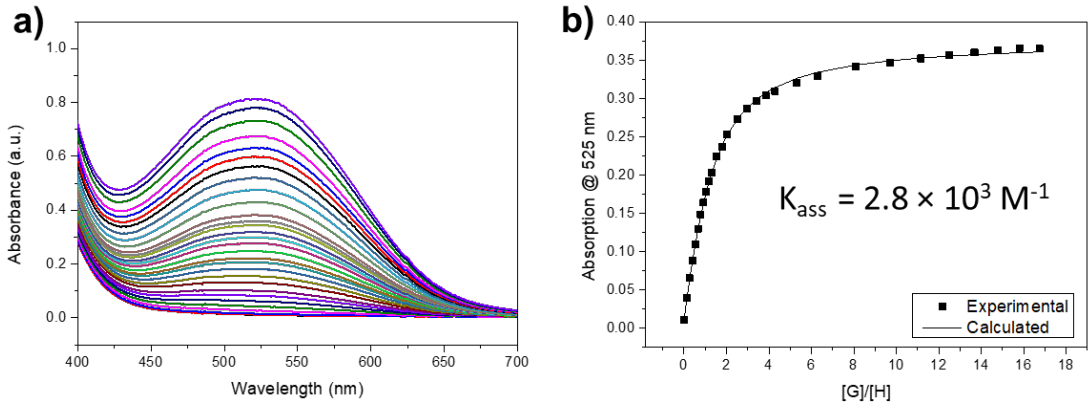

Figure 4. UV–vis and Binding curve for **L^{DNP}** (20 mM) is titrated to **ring** (500 µM) in a cuvette (1 cm). in MeCN.

Binding study **L^{DNP}** nanosphere and **ring**

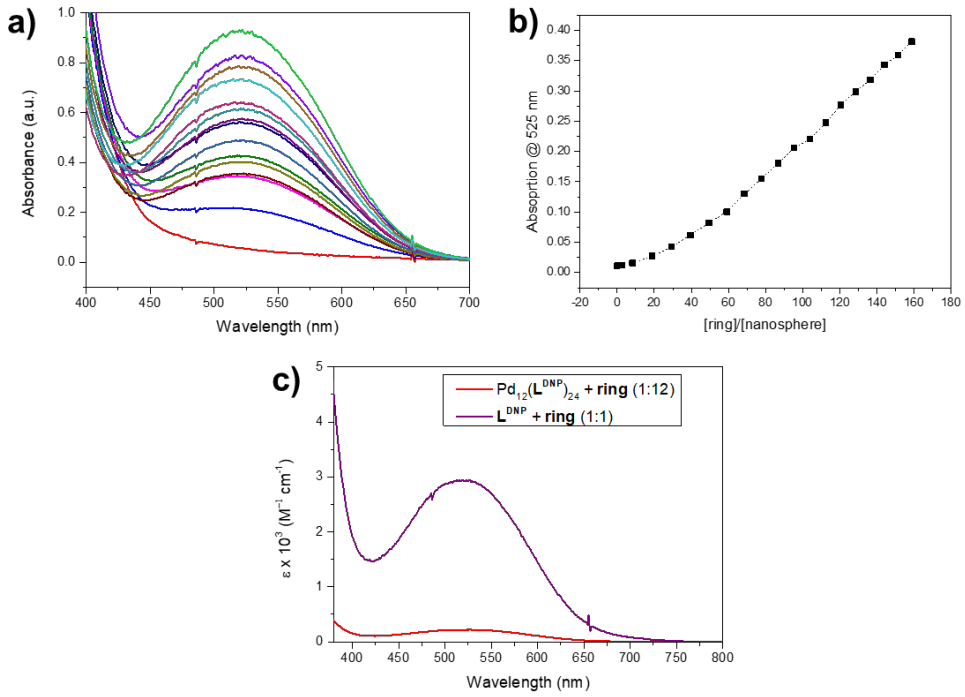

Figure 5. a) UV–vis spectra for **ring** upon titration against to **L^{DNP} nanosphere** (38.6 µM) in a cuvette (1 cm) in MeCN. b) Zoom of binding curve for **ring** (32.1 mM) is titrated to **L^{DNP} nanosphere** (38.6 µM) in a cuvette (1 cm) in MeCN. c) UV-vis spectra of 1:1 complex of **L^{DNP}:ring** pseudorotaxane 575 µM in MeCN 2 mm path length and extinction of the pseudorotaxane nanosphere 1:1 of **L^{DNP}: ring** showing an 8× lower molar absorptivity indicating a lower degree of pseudorotaxane formation.

S3. Kinetic ^{1}H NMR experiments

Calibration of nanosphere formation with ^{1}H NMR and ESI–MS

During nanosphere formation, the intensity of the pyridine peaks PyrA and PyrB increase in ^{1}H NMR over time as is shown Supplementary Figure 8, 11. Following the intensity of PyrA and PyrB over time with ^{1}H NMR matches the relative amount of nanosphere formed measured with ESI–MS. Therefore, we decided that we could follow how much nanosphere has evolved by tracking the intensity of the pyridine peaks in ^{1}H NMR. The peak intensity in ^{1}H NMR is shown relative to the intensity of PyrA and PyrB of a fully formed nanosphere sample in absence of **ring** (Supplementary Figure 6) and in presence of **ring** (Supplementary Figure 7).

The incubation period of nanosphere formation in presence of **ring** found with ESI–MS is also visible in ^{1}H NMR in Supplementary Figure 12 where a shoulder at $\Delta\delta$ = 9.03 ppm emerges after 30 minutes. This shoulder corresponds to PyrA of the pseudorotaxane nanosphere. Therefore, these curves are further used as calibration curves for how much nanosphere has evolved based on the relative peak intensity of the pyridine signal.

When nanosphere formation is performed at 0°C in absence of **ring** (Supplementary Figure 9), only broad pyridine signals are observed, and no difference is observed in all measured spectra over a 14-hour time course. This implies that the Pd–L polymer is formed that does not convert into nanospheres. Nanosphere formation in presence of **ring** at 0°C (Supplementary Figure 13) also shows no difference is observed in all measured spectra over a 14-hour time course. Moreover, no shoulder emerges at the resonance at $\Delta\delta$ = 9.03 ppm, indicating that there is no pseudorotaxane nanosphere formation at this temperature. At 10°C, this peak shoulder corresponding to the nanosphere pyridine signal emerges (Supplementary Figure 14 & 15), indicating that there is 12% conversion towards the pseudorotaxane-nanosphere according to the calibration curve

(Supplementary Figure 7). Conversely, in absence of **ring** no nanosphere emerges at 10°C as no difference is observed in all measured ^{1}H NMR spectra represented in Supplementary Figure 10.

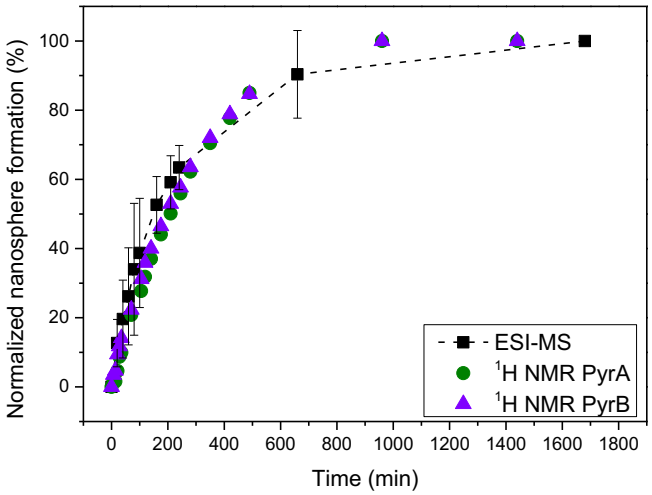

Figure 6. Calibration curve for normalized nanosphere formation over time in absence of **ring** (Pathway 1) measured with ESI–MS (black squares) and ^{1}H NMR by tracking the intensity of the PyrA (9.14 ppm, green circles) and PyrB (8.03 ppm, purple triangles) (Supplementary Figure 3a). As both methods show the same result, we can use the pyridine peak intensity to determine how much $Pd_{12}(\mathbf{L}^{\mathbf{DNP}})_{24}$ nanosphere has formed.

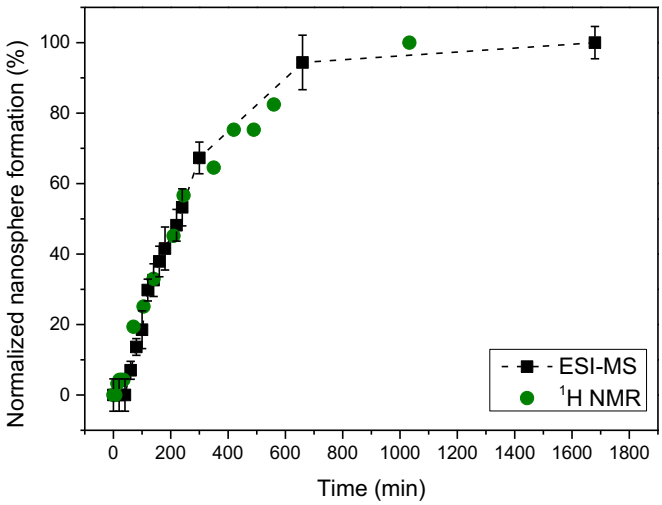

Figure 7. Calibration curve for normalized pseudorotaxane-nanosphere formation over time in presence of **ring** (Pathway 2) measured with ESI–MS (black squares) and ^{1}H NMR (green circles) by tracking the intensity of the PyrA at $\Delta\delta$ = 9.03 ppm (Supplementary Figure 3c). As both methods show the same result, we can use the pyridine peak intensity to determine how much $Pd_{12}(\mathbf{L}^{\mathbf{DNP}})_{24}(\mathbf{ring})_{8\pm5}$ nanosphere has formed.

The error bars shown for the ESI–MS data are based on the counts for the signals of the nanospheres for $[\mathbf{Pd_{12}(L^{DNP})_{24}](BF_4)_n}^{7–9+}$ and $[\mathbf{Pd_{12}(L^{DNP})_{24}(ring)_m(BF_4)_n(PF_6)_{24-n}}]^{9–11+}$ (Supplementary Figure 28 & 29). The final intensity for all nanosphere peaks at time = 1680 min was set at 100% and all other intensities found overtime were normalized to this value.

Monitoring the self-assembly assembly

The $\mathbf{L^{MeO}}$ building block featuring minimal *exo*-functionalization (Figure 2) was employed to explore the kinetics of $Pd_{12}(\mathbf{L^{MeO}})_{24}$ nanosphere formation and enable identification of the resting-state.[10] During the self-assembly process of nanospheres based on $\mathbf{L^{MeO}}$ ligands, size changes of intermediate species was monitored by DOSY ^{1}H NMR (via $\mathbf{L^{MeO}}$ pyridine resonances) to reveal differences, giving insight into the temporal evolution of products and intermediate structures via the diffusion constant (Log*D*, Figure 2b). The diffusion of the free $\mathbf{L^{MeO}}$ ligand (Log*D* = -8.66) decreases upon addition of 0.52 Equiv. of Pd^{2+}, indicative of the rapid formation of a large species (Log*D* = -9.66) within the first 20 minutes of the experiment. Over a 17-hour time-course, the diffusion gradually increases again to a final value of (Log*D* =-9.46), in line with the formation of the $Pd_{12}(\mathbf{L^{MeO}})_{24}$ nanosphere (Supplementary Table 1).[10] This experiment shows that nanosphere assembly proceeds via the rapid formation of a large species, identified as the **Pd**–$\mathbf{L^{MeO}}$ coordination polymer (i.e., Pd–L polymer), acting as an intermediate state from which nanospheres slowly evolve (Figure 2).

Having identified that the pathway for nanosphere formation proceeds via a Pd–L polymer, proceeds via a Pd–L polymer, we explored strategies to attenuate the kinetic pathway of self-assembly by designing building blocks that would target destabilization of this specific intermediate, as it represents a resting-state that lies before the rate determining step. Thus, engineering destabilization-ability into this Pd–L polymer intermediate may serve as an impetus for rate enhancements. Consequently, this approach of pathway engineering would enable us to realize a route for nanosphere self-assembly that is catalytic in nature.

We envisioned that the use of electrostatic repulsion between the building blocks can be employed to destabilize the large Pd–L polymer, but this interaction should be realized in a reversible (i.e.,

switchable) fashion. To this end, we designed the $\mathbf{L}^{\mathbf{DNP}}$ building block, featuring a 1,5-dihydroxynaphthalene (**DNP**) recognition site for reversible binding of the charged **ring** via formation of the $\mathbf{L}^{\mathbf{DNP}}\subset\mathbf{ring}$ pseudorotaxane (chemical structures in Figure 3b).[11–13] The presence of **ring** is envisaged to induce charge accumulation on the Pd–$\mathbf{L}^{\mathbf{DNP}}$ polymer, destabilizing this intermediate resting-state. Consequently, the binding of **ring** to the Pd–$\mathbf{L}^{\mathbf{DNP}}$ steers the system an alternative kinetic trajectory, thereby acting as a kinetic controller.

Therefore, we interrogated the nanosphere-formation phenomena of $Pd_{12}(\mathbf{L}^{\mathbf{DNP}})_{24}$ in the presence and absence of **ring**. Depicted in Figure 3a, these pathways respectively yield either nanosphere (partially) *exo*-decorated with $\mathbf{L}^{\mathbf{DNP}}\subset\mathbf{ring}$ pseudorotaxanes (Pathway 2) or the parent $M_{12}(\mathbf{L}^{\mathbf{DNP}})_{24}$ nanosphere (Pathway 1). Fortuitously, pseudorotaxane formation and nanosphere assembly are established to be orthogonal.[4–7] Notably, the electrostatic interaction between **ring** and *endo*-functionalized $Pd_{12}L^{\alpha}_{24}$ nanospheres has previously been explored by Stoddart, Fujita and coworkers.[14], where L^{α} is ditopic bis(pyridyl) ligand featuring a **DNP** unit. The binding of the **ring** is reversible in both our design and the reported example (according to Figure 3a).

Nanosphere formation via Pathway 1

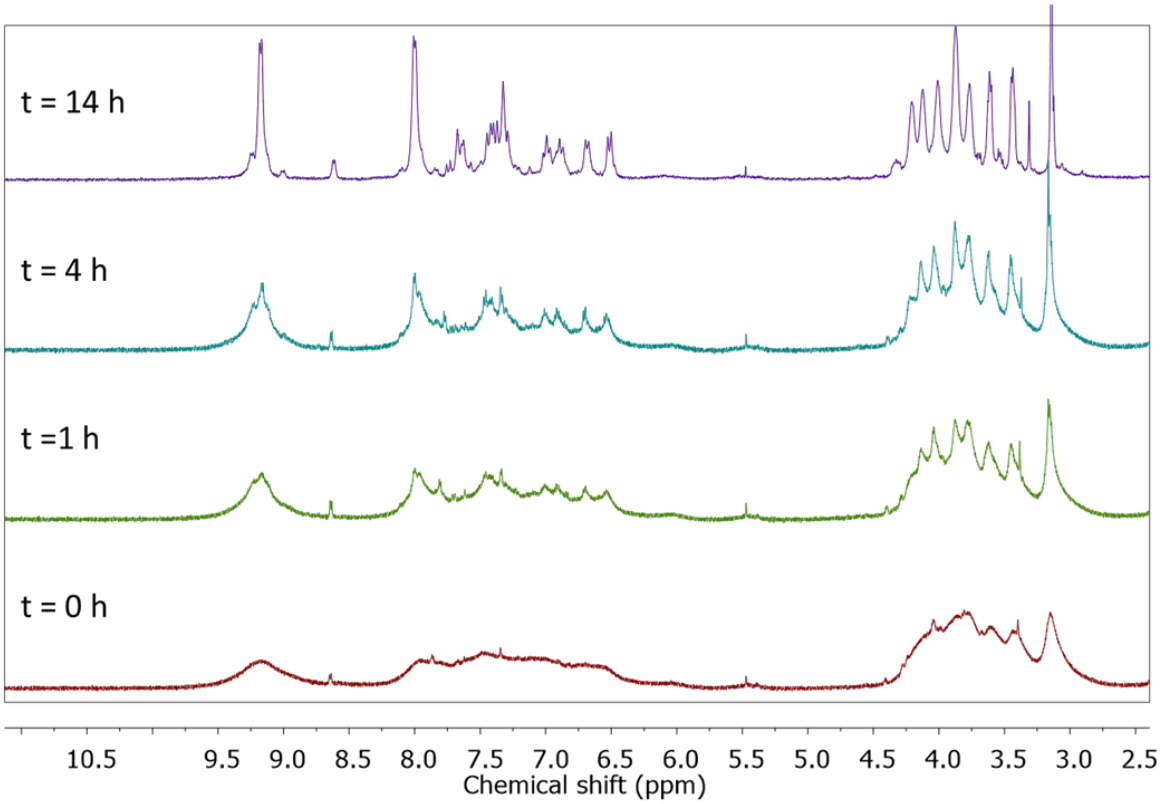

Figure 8. Selection of ^{1}H NMR spectra of $Pd_{12}(\mathbf{L}^{\mathbf{DNP}})_{24}$ nanosphere formation in absence of **ring** at t = 0 h (red) t = 14 h at 25°C (purple) showing that the pyridine signals at $\Delta\delta$ = 9.17 ppm and $\Delta\delta$ = 8.00 ppm become more narrow, more intense and more defined over time. ^{1}H NMR spectra were recorded every 10 minutes.

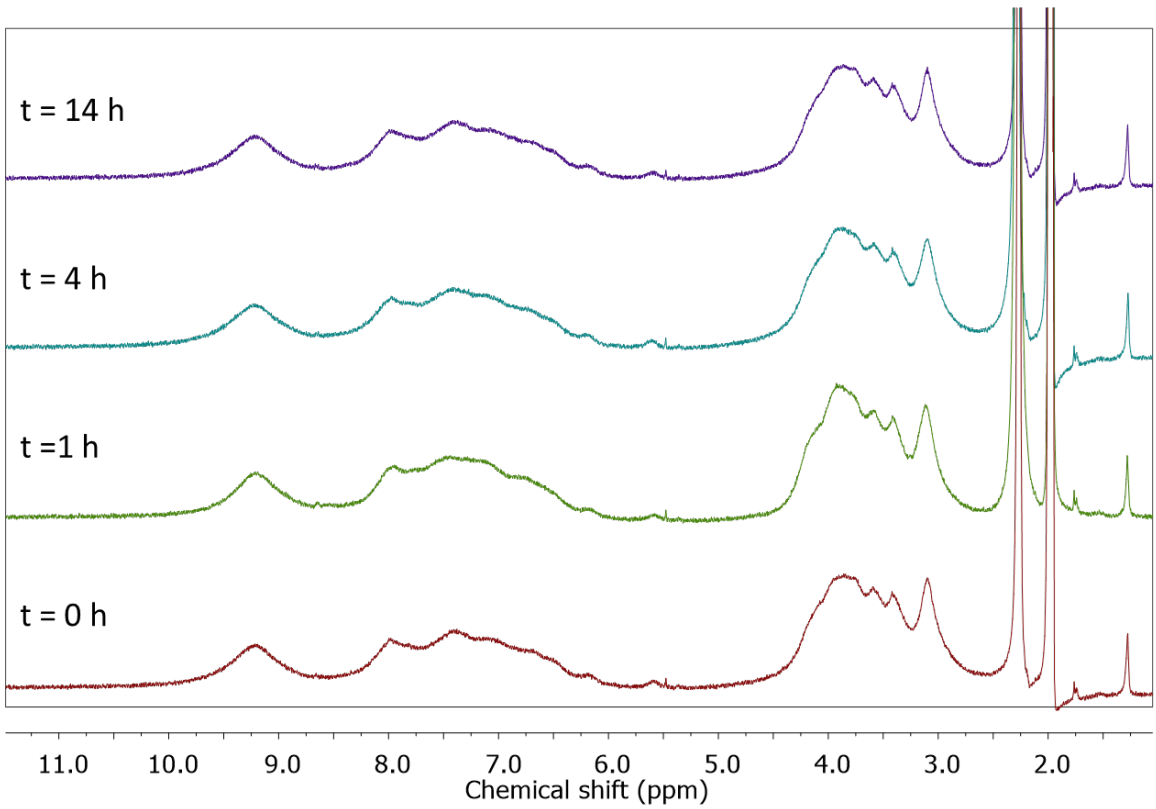

Figure 9. Selection of ^{1}H NMR spectra of Pd–L polymer between $\mathbf{L}^{\mathbf{DNP}}$ and Pd^{2+} over time at 0°C from t = 0 h in (red) to t = 14 h (purple) showing no change of the pyridine signals at $\Delta\delta$ = 9.17 ppm and $\Delta\delta$ = 8.00 ppm indicating that there is no $Pd_{12}(\mathbf{L}^{\mathbf{DNP}})_{24}$ nanosphere formation. ^{1}H NMR spectra were recorded every 10 minutes.

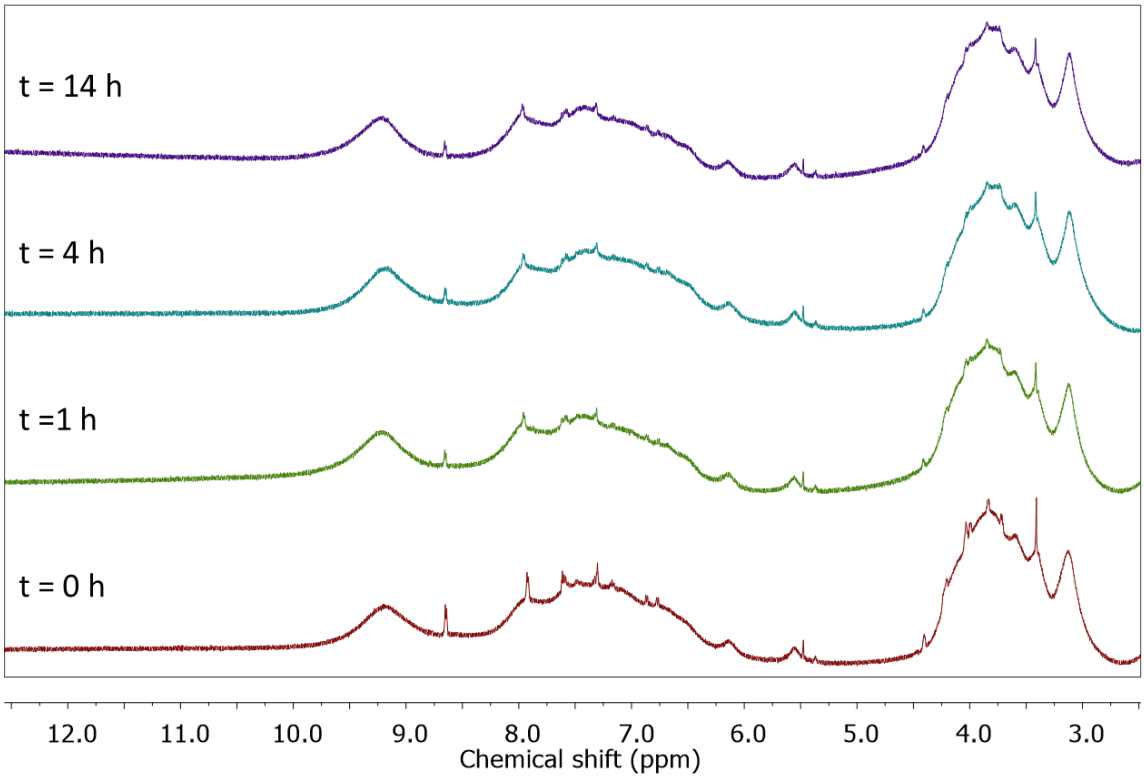

Figure 10. Selection of ^{1}H NMR spectra of Pd–L polymer between $\mathbf{L}^{\mathbf{DNP}}$ and Pd^{2+} over time at 10°C from t = 0 h in (red) to t = 14 h (purple) showing no change of the pyridine signals at $\Delta\delta$ = 9.17 ppm and $\Delta\delta$ = 8.00 ppm indicating that there is no $Pd_{12}(\mathbf{L}^{\mathbf{DNP}})_{24}$ nanosphere formation. ^{1}H NMR spectra were recorded every 10 minutes.

Nanosphere formation via Pathway 2

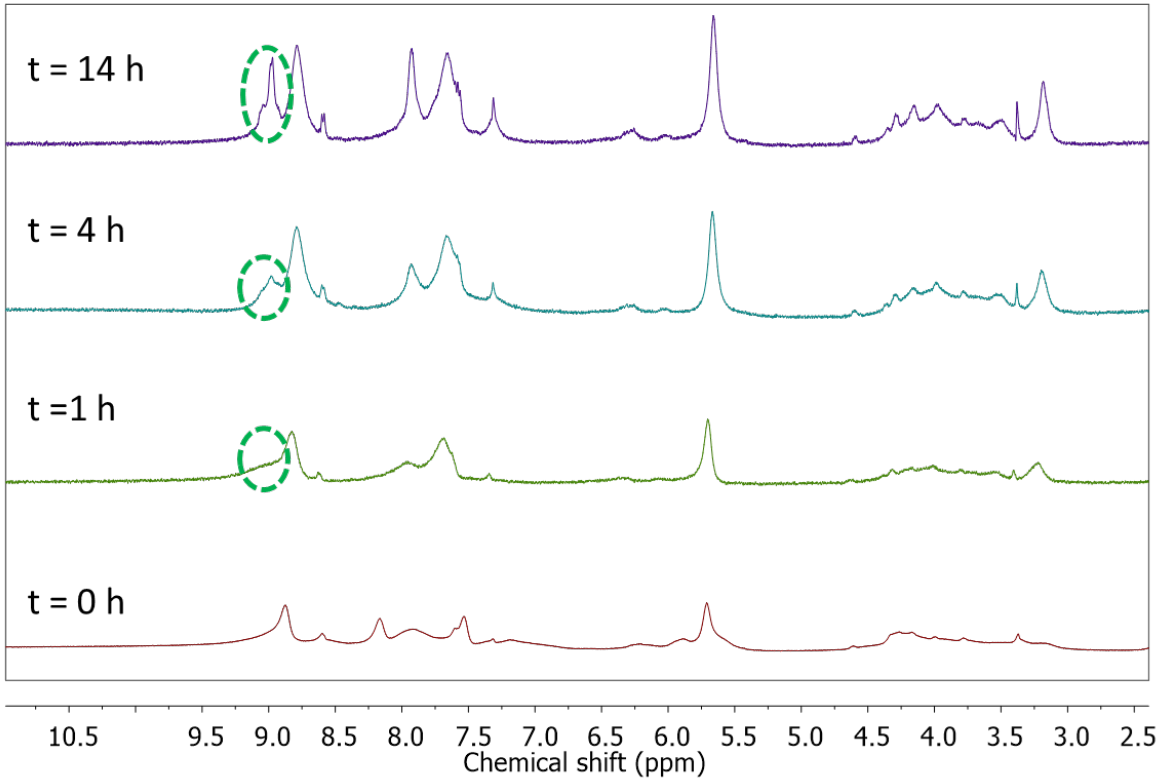

Figure 11. Selection of ^{1}H NMR spectra of pseudorotaxane-nanosphere formation in presence of **ring** over time at 25°C from t = 0 h in (grey) to t = 14 h (purple) showing that the pyridine resonances at $\Delta\delta$ = 9.03 ppm & $\Delta\delta$ = 7.99 ppm become more narrow, more intense and more defined over time. ^{1}H NMR spectra were recorded every 10 minutes.

Emergence of $Pd_{12}(\mathbf{L}^{DNP})_{24}(\mathbf{ring})_{8\pm5}$ nanosphere resonance @ $\Delta\delta$ = 9.03 ppm

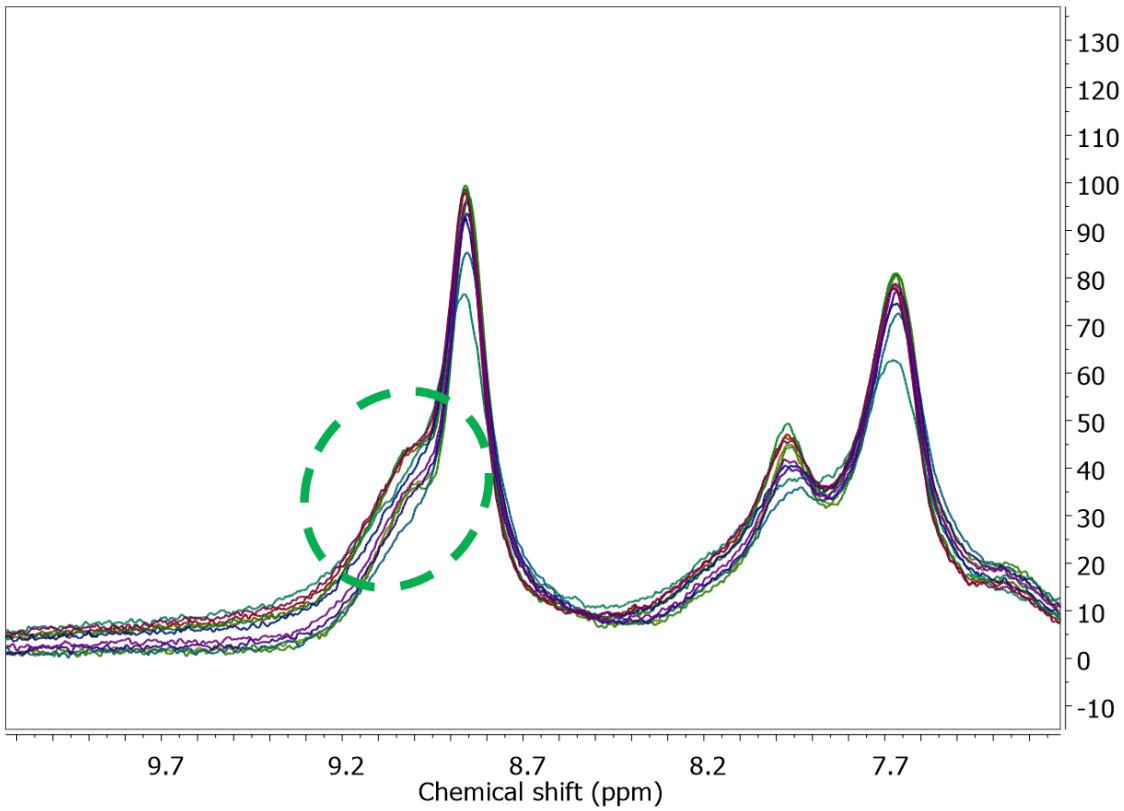

Figure 12. Selection of ^{1}H NMR spectra for pseudorotaxane-nanosphere formation in presence of **ring** over time at 25°C from t = 0 h in (turquoise) to t = 30 minutes (red) showing the emergence of a shoulder at $\Delta\delta$ = 9.03 ppm, the pyridine signal after 15 minutes, the incubation period. ^{1}H NMR spectra were recorded every 5 minutes.

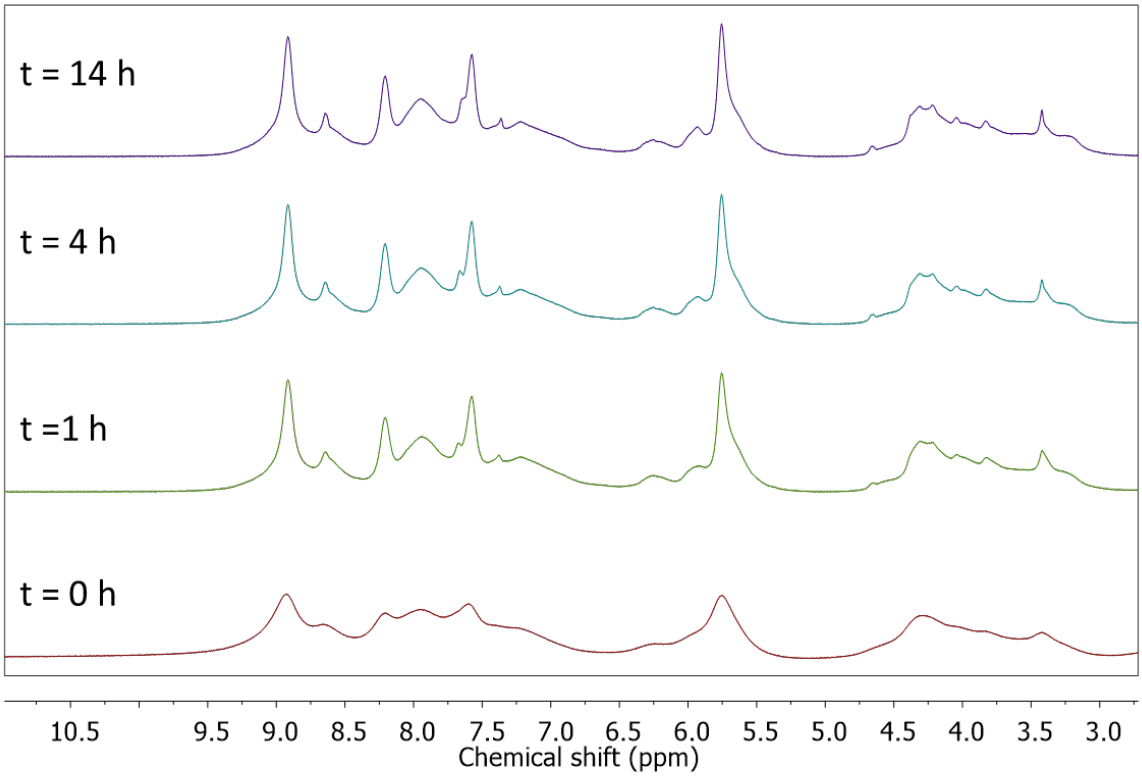

Figure 13. Selection of ^{1}H NMR spectra of coordination oligomer formed between **ring**, $\mathbf{L}^{\mathbf{DNP}}$ and Pd^{2+} over time at 0°C from t = 0 h in (red) to t = 14 h (purple) showing no change in all measured spectra. The absence of a resonance at $\Delta\delta$ = 9.03 ppm indicates that there is no $Pd_{12}(\mathbf{L}^{\mathbf{DNP}})_{24}(\mathbf{ring})_{8\pm5}$ nanosphere formation. ^{1}H NMR spectra were recorded every 10 minutes.

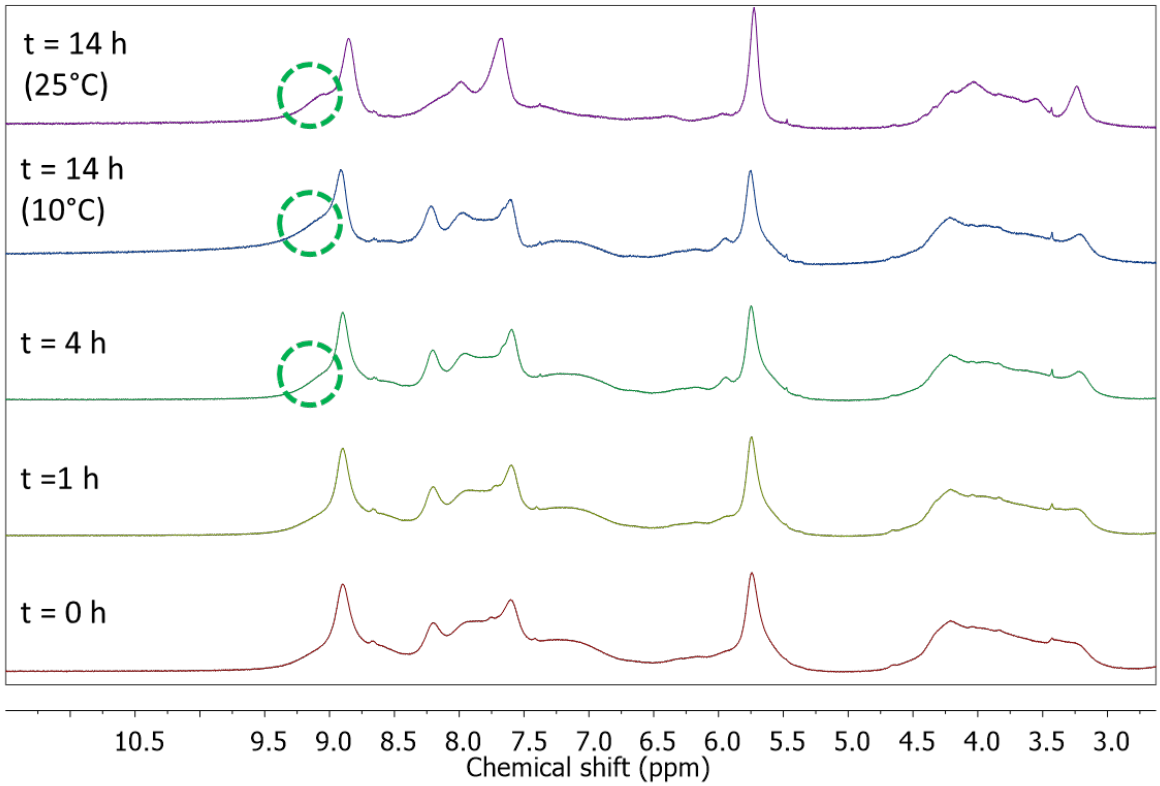

Figure 14. Selection of ^{1}H NMR spectra of pseudorotaxane nanosphere formation in presence of **ring** over time at 10°C from t = 0 h in (red) to t = 14 h (purple). The spectra show the emergence of a shoulder resonance at $\Delta\delta$ = 9.03 ppm corresponding to the pyridine signal of the $Pd_{12}(\mathbf{L}^{\mathbf{DNP}})_{24}(\mathbf{ring})_{8\pm5}$ nanosphere. Using the calibration curve of Supplementary Figure 7 this indicates that there is 12% conversion towards pseudorotaxane nanosphere. ^{1}H NMR spectra were recorded every 10 minutes. The ^{1}H NMR after 14 hours was measured at 10°C and at 25°C to allow for a fair comparison to the NMR data that was used to construct the calibration curve 25°C.

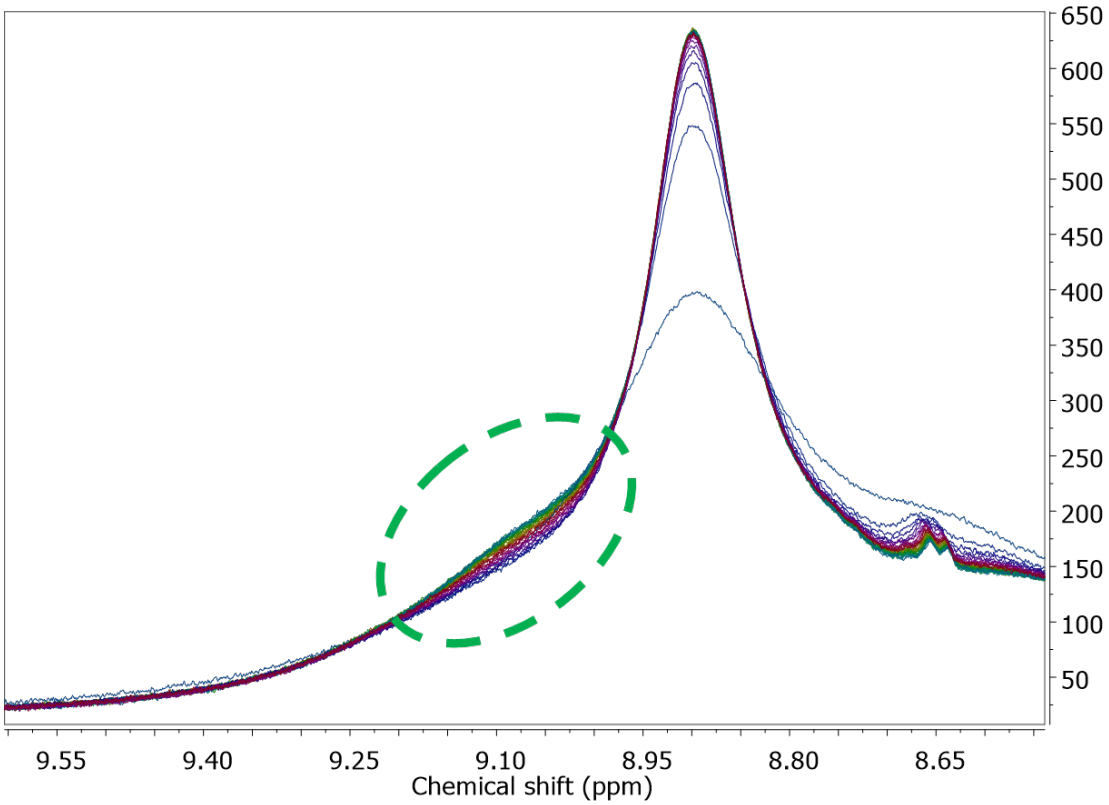

Figure 15. Selection of ^{1}H NMR spectra of pseudorotaxane nanosphere formation in presence of **ring** over time at 10°C from t = 0 h in (red) to t = 14 h (blue) showing the emergence of a shoulder resonance at $\Delta\delta$ = 9.03 ppm corresponding to the pyridine signal of the $Pd_{12}(\mathbf{L}^{\mathbf{DNP}})_{24}(\mathbf{ring})_{8\pm5}$.nanosphere.

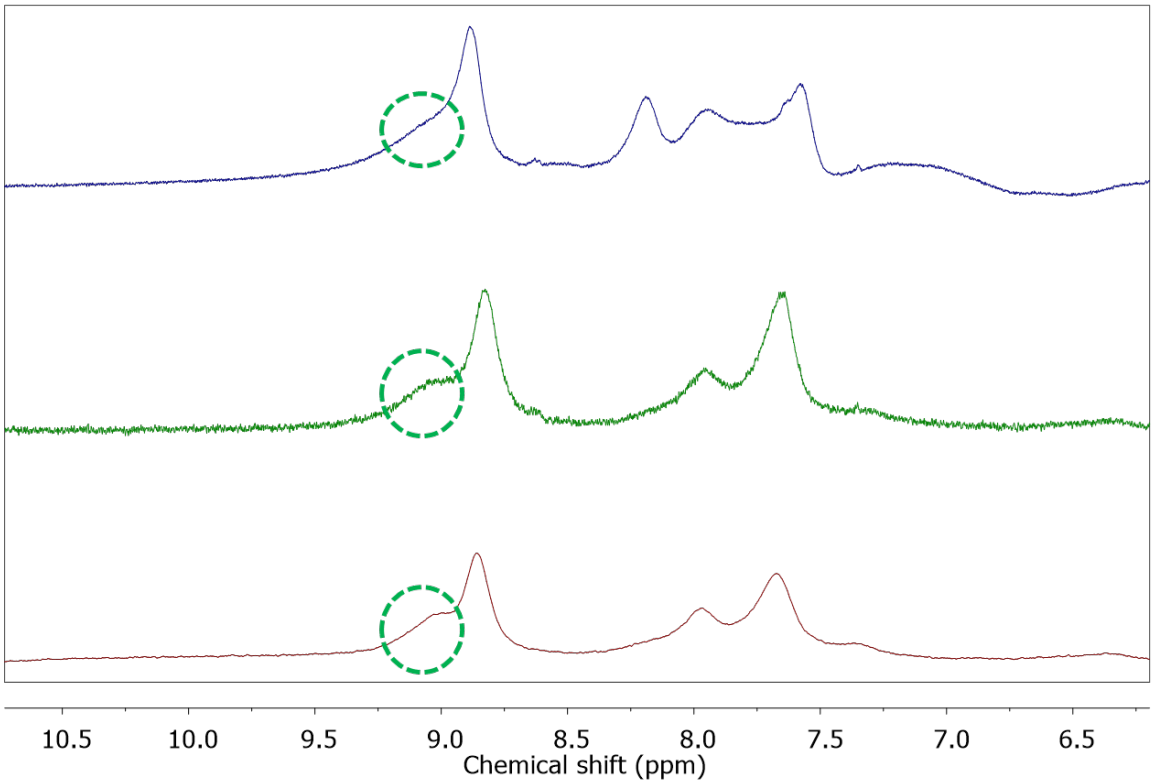

Figure 16. ^{1}H NMR spectra of pseudorotaxane nanosphere formation in presence of **ring** after 14 hours measured at 10°C (blue) and measured at 25°C (black). The ^{1}H NMR spectrum (red) of nanosphere formation at 25°C used to construct the calibration curve at t = 80 minutes corresponding to 12% nanosphere formation. The red and the black spectrum overlapping was used to determine nanosphere formation for every point in time a 10°C.

S4. Kinetic switching experiment

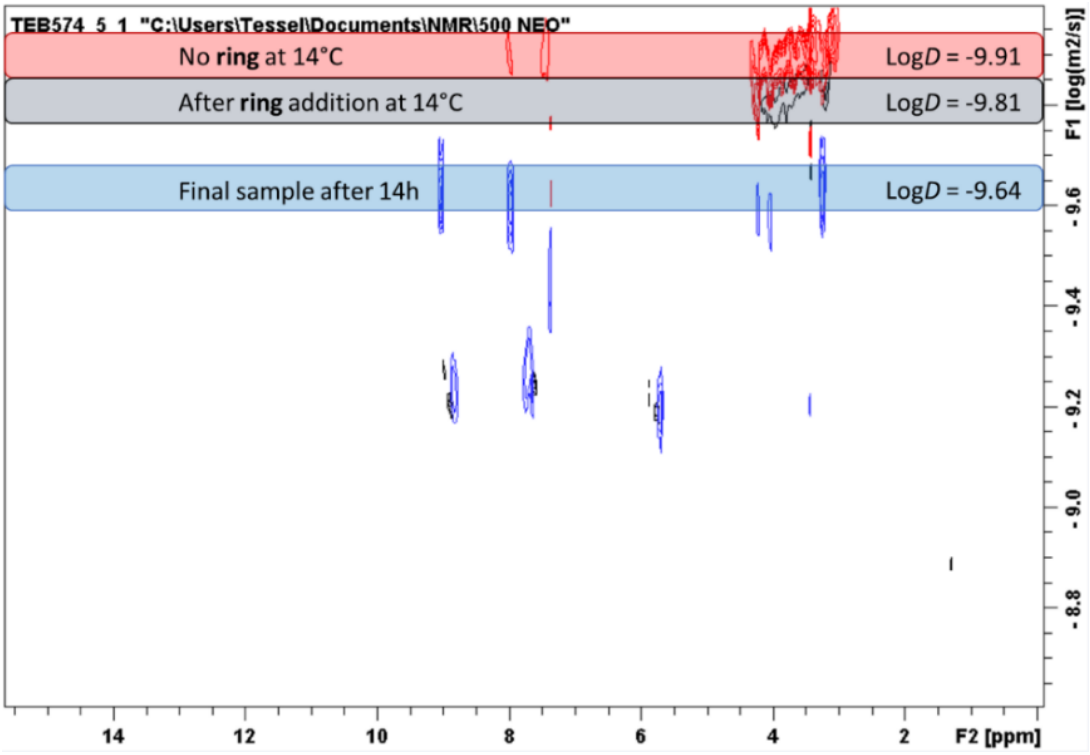

Figure 17. DOSY ^{1}H NMR spectra kinetic pathway switching experiment conducted at 14°C. DOSY spectrum of the large Pd–L polymer in red shows a low diffusion constant (Log*D* = -9.91). After 30 minutes **ring** is added showing that immediately a higher diffusion constant (Log*D* = -9.81) (black) indicating the formation of smaller coordination clusters. Overnight, the pseudorotaxane–nanosphere is formed, indicated by the diffusion constant (Log*D* = -9.64) (blue).

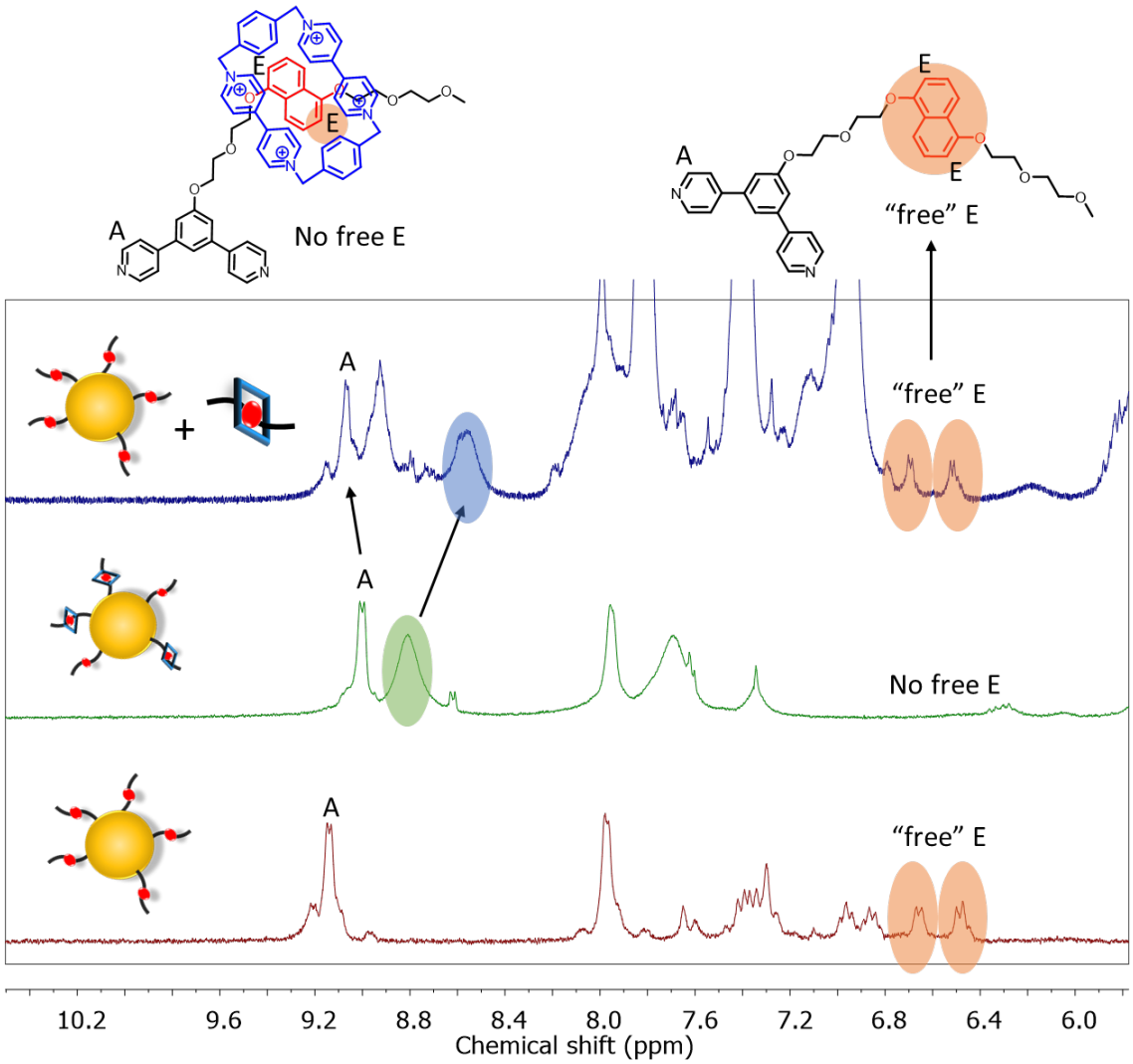

Figure 18. ^{1}H NMR of nanosphere in absence of **ring** (red) with the characteristic resonances of the **DNP** moiety (resonance "E" ~6.5–6.7 ppm) of ligand $\mathbf{L}^{\mathbf{DNP}}$ that comprises the $Pd_{12}(\mathbf{L}^{\mathbf{DNP}})_{24}$ cage. In the presence of **ring** (green) the "free" E resonance experiences an downfield shift upon pseudorotaxane formation. The addition of competing **DNP** Guest (blue) to the solution leads to exchange, entailing dethreading of **ring** from the $Pd_{12}(\mathbf{L}^{\mathbf{DNP}})_{24}(\mathbf{ring})_{8\pm5}$. Nanosphere and subsequent pseudorotaxane formation with the competing DNP guest (blue). The blue trace reveals the subsequent shift of PyrA from the "parent" $Pd_{12}(\mathbf{L}^{\mathbf{DNP}})_{24}$ nanosphere coinciding with the emergence of "free" E proton resonance of the **DNP** moiety in the $\mathbf{L}^{\mathbf{DNP}}$ of $Pd_{12}(\mathbf{L}^{\mathbf{DNP}})_{24}$. The unbinding of **ring** from the $\mathbf{L}^{\mathbf{DNP}}$ in the nanosphere leads to the emergence of the free naphthalene proton E, clearly visible in the blue spectrum upon comparison to the red spectrum.

S5. Control experiments for the ring acting as kinetic controller

To demonstrate that the observed effects of the ring acting as kinetic controller required pseudorotaxane formation and were not a result of change in polarity of the solvent or ionic strength, a control experiment was performed using methyl viologen bis(hexafluorophosphate) (**MV**($\mathbf{PF_6}$)$_2$) as a model for the **ring** structure.

- Upon mixing **MV**($\mathbf{PF_6}$)$_2$ and $\mathbf{L^{DNP}}$ (2:1) no shifts or signal broadening were observed in ^{1}H NMR, confirming the lack of interaction between these two molecules.
- Upon addition of Pd^{2+} a precipitate was observed, identified as the coordination polymer formed between $\mathbf{L^{DNP}}$ and Pd^{2+}(Supplementary Figure 19). In this case, no nanosphere formation was observed. $\mathbf{L^{MeO}}$ nanospheres formation in presence of **ring** was monitored by DOSY ^{1}H NMR, demonstrating presence of the Pd–L polymer intermediate.

Accordingly, these results imply that **ring** has no effect on nanosphere formation kinetics if the ligand has no binding site for **ring**. These control experiments indicate that the observed difference between Pathway 1 and 2 is not simply an ion effect or an effect caused by presence of the pyridinium structure of **ring** or **MV**. Instead, this difference in behavior arises from the supramolecular interaction between the **ring**, $\mathbf{L^{DNP}}$ and the Pd^{2+} within the system, from which pseudorotaxane formation can control the kinetic trajectory of nanosphere assembly (i.e., **ring** acts as kinetic controller).

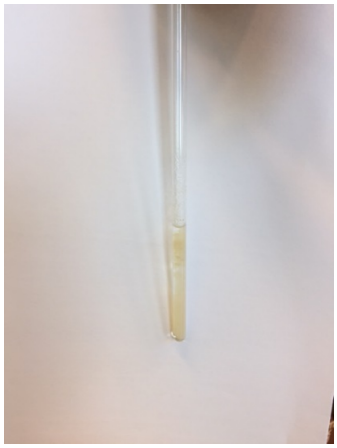

Figure 19. NMR tube containing $\mathbf{L^{DNP}}$ and $\mathbf{MV(PF_6)_2}$ to which just Pd^{2+} has been added, resulting in a precipitation.

S6. ESI–MS steady state of nanosphere formation Pathway 1 and 2

ElectroSpray Ionization High Resolution Mass Spectrometry (ESI–HRMS).

Mass spectra were collected on a HR-ToF Bruker Daltonik GmbH (Bremen, Germany) Impact II, an ESI–ToF MS capable of resolution of at least 40000 FWHM. Detection was in positive-ion mode and the source voltage was between 4 and 6 kV. The sample was introduced with a syringe pump at a flow rate of 18 μL hr^{-1}. The drying gas (N_2) was held at 180°C. The machine was calibrated prior to every experiment via direct infusion of a TFA-Na solution, which provided a *m/z* range of singly charged peaks up to 3500 Da in both ion modes. Software acquisition Compass 2.0 for Otof series. Software processing Compass DataAnalysis 4.0 sri (x64). Both Bruker Daltonik GmbH (Bremen, Germany). Processing of the displayed spectra was further performed using the mMass software, all spectra were averaged and baseline corrected.

S6.1. ESI–MS for nanosphere sample [$Pd_{12}(L^{DNP})_{24}(BF_4)_{24}$]

Table 2. Different species of **[$Pd_{12}(L^{DNP})_{24}(BF_4)_n$]** nanosphere sample observed with ESI–MS and corresponding calculated *m/z*. The expanded spectrum for different charged species and simulated isotope distribution is similar to Supplementary Figure 21.

Species	Charge	Found (*m/z*)	Calculated (*m/z*)
[$Pd_{12}(L^{DNP})_{24}(BF_4)_{10}$]	14^+	1148.6499	1148.6490
[$Pd_{12}(L^{DNP})_{24}(BF_4)_{11}$]	13^+	1243.7008	1243.6994
[$Pd_{12}(L^{DNP})_{24}(BF_4)_{12}$]	12^+	1354.5084	1354.5079
[$Pd_{12}(L^{DNP})_{24}(BF_4)_{13}$]	11^+	1485.5550	1485.5545
[$Pd_{12}(L^{DNP})_{24}(BF_4)_{14}$]	10^+	1642.8114	1642.8103
[$Pd_{12}(L^{DNP})_{24}(BF_4)_{15}$]	9^+	1835.0128	1835.0119
[$Pd_{12}(L^{DNP})_{24}(BF_4)_{16}$]	8^+	2075.1395	2075.1390
[$Pd_{12}(L^{DNP})_{24}(BF_4)_{17}$]	7^+	2384.0163	2384.0165
[$Pd_{12}(L^{DNP})_{24}(BF_4)_{18}$]	6^+	2795.8473	2795.8535

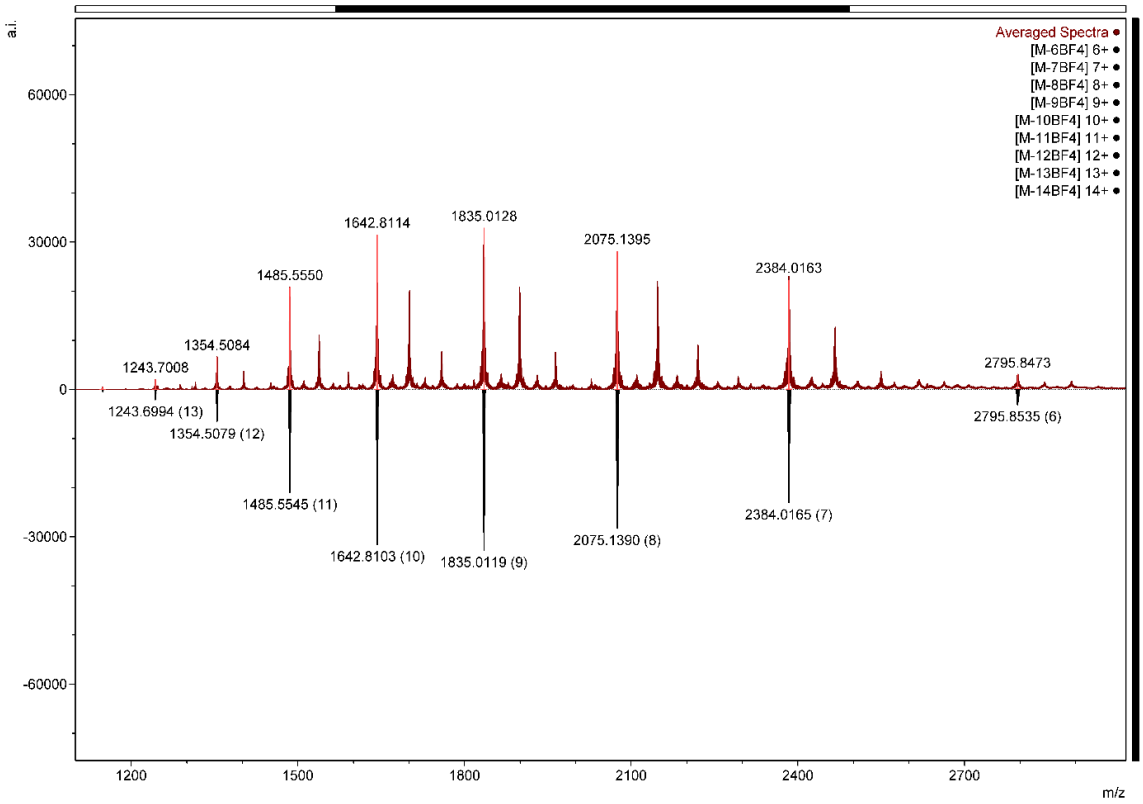

Figure 20. Full ESI–MS for nanosphere sample **[$Pd_{12}(L^{DNP})_{24}(BF_4)_{24}$]**.

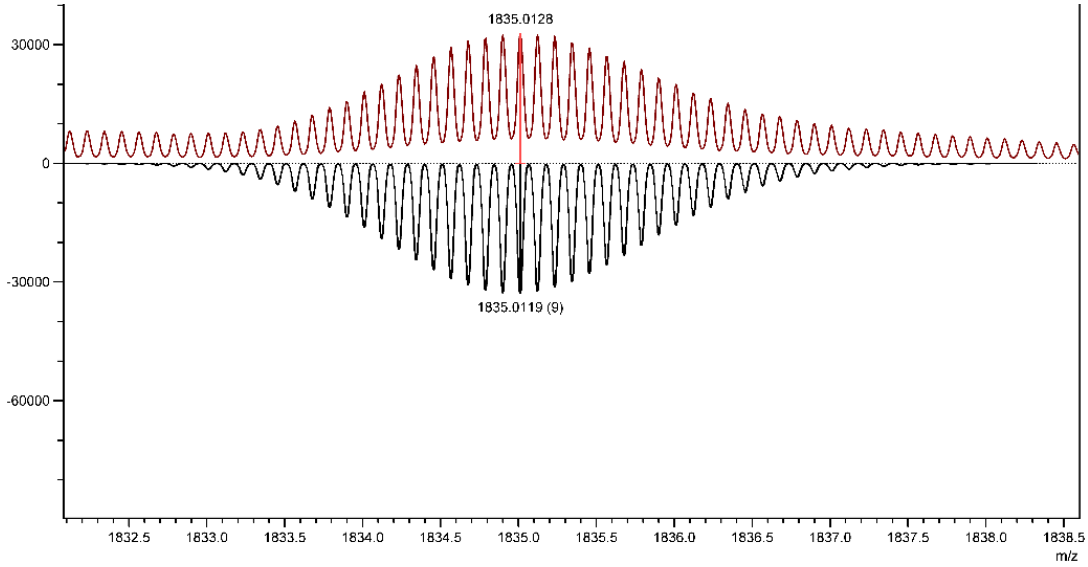

Figure 21. ESI–MS signal for $[Pd_{12}(\mathbf{L^{DNP}})_{24}(BF_4)_{15}]^{9+}$, *m/z* = 1835.0128, calculated *m/z* = 1835.0119.

S6.2. ESI–MS for nanosphere sample [$Pd_{12}(L^{DNP})_{24}(ring)_m(BF_4)_n(PF_6)_{24-n}$]

Table 3. Different species of **[$Pd_{12}(L^{DNP})_{24}(ring)_m(BF_4)_n(PF_6)_{24-n}$]** nanosphere sample observed with ESI–MS and corresponding calculated *m/z*. The expanded spectrum for different charged species and simulated isotope distribution are similar to Supplementary Figure 23 and Supplementary Figure 24.

Species	Charge	Found (*m/z*)	Calculated (*m/z*)
[$Pd_{12}(L^{DNP})_{24}(BF_4)_5(PF_6)_6$]	13^+	1270.5270	1270.5273
[$Pd_{12}(L^{DNP})_{24}(BF_4)_5(PF_6)_7$]	12^+	1388.4846	1388.4849
[$Pd_{12}(L^{DNP})_{24}(BF_4)_5(PF_6)_8$]	11^+	1527.8886	1527.8895
[$Pd_{12}(L^{DNP})_{24}(BF_4)_5(PF_6)_9$]	10^+	1695.1735	1695.1749
[$Pd_{12}(L^{DNP})_{24}(BF_4)_5(PF_6)_{10}$]	9^+	1899.6324	1899.6348
[$Pd_{12}(L^{DNP})_{24}(BF_4)_5(PF_6)_{11}$]	8^+	2155.2111	2155.2097
[$Pd_{12}(L^{DNP})_{24}(BF_4)_5(PF_6)_{12}$]	7^+	2483.8195	2483.8061
[$Pd_{12}(L^{DNP})_{24}(ring)_1(BF_4)_5(PF_6)_{16}$]	11^+	1617.3633	1617.3622
[$Pd_{12}(L^{DNP})_{24}(ring)_1(BF_4)_5(PF_6)_{17}$]	10^+	1793.5935	1793.5948
[$Pd_{12}(L^{DNP})_{24}(ring)_1(BF_4)_5(PF_6)_{18}$]	9^+	2008.9912	2008.9903
[$Pd_{12}(L^{DNP})_{24}(ring)_1(BF_4)_5(PF_6)_{19}$]	8^+	2278.2395	2278.2346

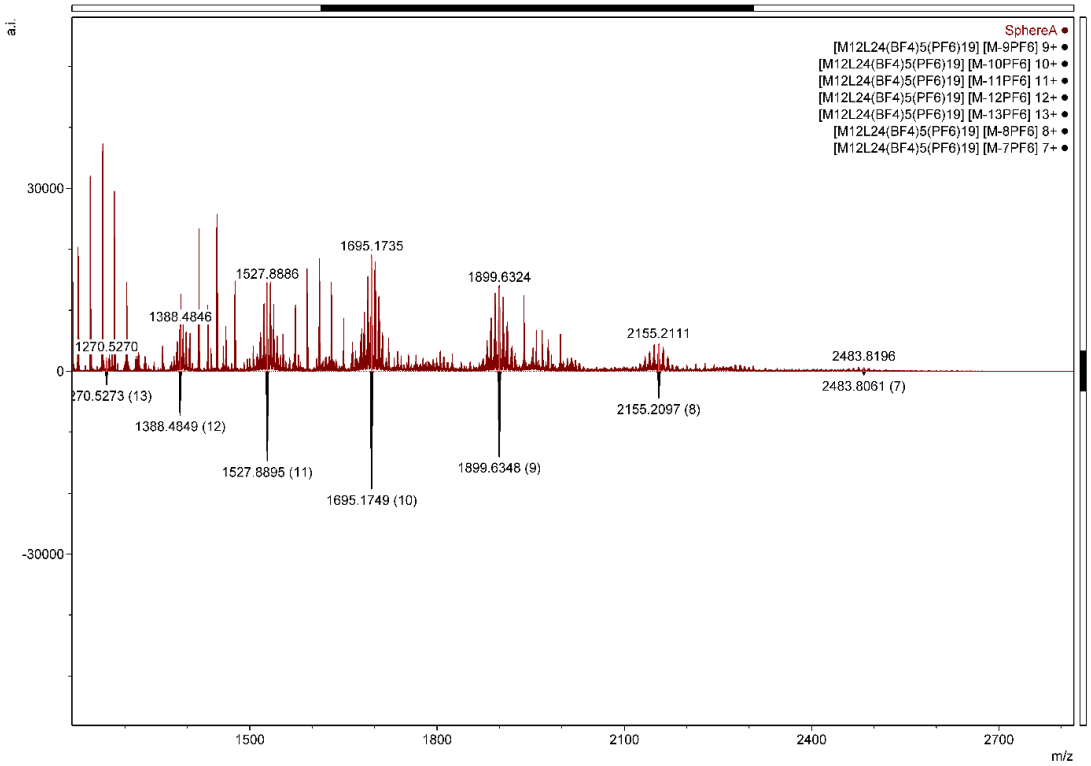

Figure 22. Full ESI–MS for nanosphere sample $\mathbf{[Pd_{12}(L^{DNP})_{24}(ring)_m(BF_4)_n(PF_6)_{24-n}]}$.

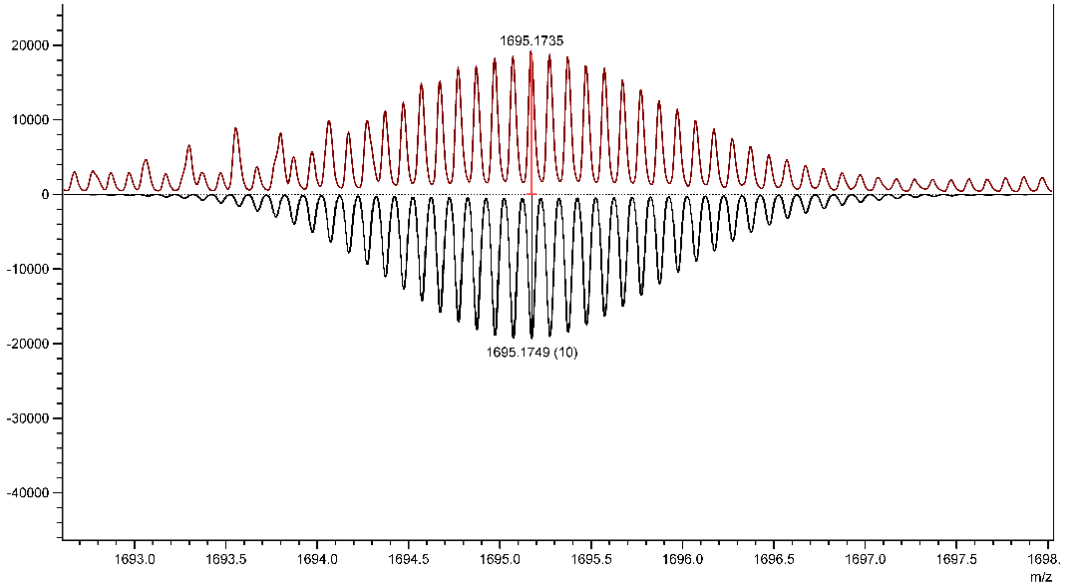

Figure 23. ESI–MS peak for $\mathbf{[Pd_{12}(L^{DNP})_{24}(BF_4)_5(PF_6)_9]^{10+}}$, m/z = 1695.1735, calculated m/z = 1695.1749.

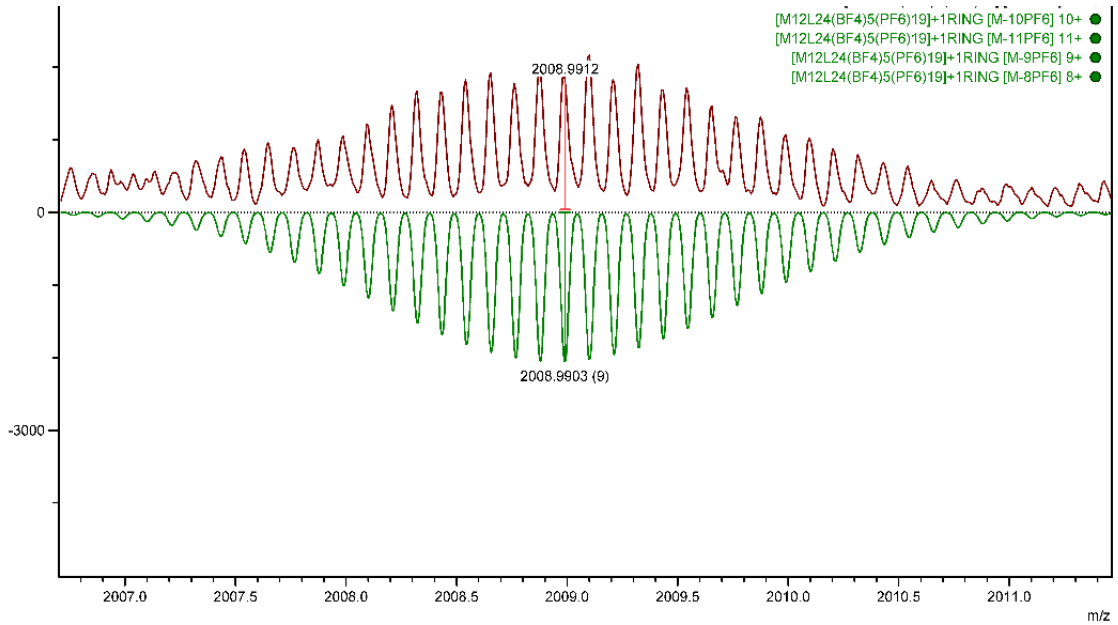

Figure 24. ESI–MS peak for $\mathbf{[Pd_{12}(L^{DNP})_{24}(ring)_1(BF_4)_5(PF_6)_{18}]^{9+}}$, m/z = 2008.9912, calculated m/z = 2008.9903.

S6.3. ESI–MS for nanosphere sample [$Pd_{12}(L^{DNP})_{24}(ring)_m(PF_6)_{4\cdot m+24}$]

Table 4. Different species of **[$Pd_{12}(L^{DNP})_{24}(ring)_m(PF_6)_{4\cdot m+24}$]** nanosphere sample observed with ESI–MS and corresponding calculated *m/z*. The expanded spectrum for different charged species and simulated isotope distribution are similar to Supplementary Figure 26.

Species	Charge	Found (*m/z*)	Calculated (*m/z*)
[$Pd_{12}(L^{DNP})_{24}(ring)_4(PF_6)_{32}$]	8^+	2741.6971	2741.7455
[$Pd_{12}(L^{DNP})_{24}(ring)_4(PF_6)_{31}$]	9^+	2420.9608	2420.9997
[$Pd_{12}(L^{DNP})_{24}(ring)_5(PF_6)_{36}$]	8^+	2879.3411	2879.3856
[$Pd_{12}(L^{DNP})_{24}(ring)_5(PF_6)_{35}$]	9^+	2543.3044	2543.3467
[$Pd_{12}(L^{DNP})_{24}(ring)_6(PF_6)_{40}$]	8^+	3016.8486	3016.9007
[$Pd_{12}(L^{DNP})_{24}(ring)_6(PF_6)_{39}$]	9^+	2665.5403	2665.5823
[$Pd_{12}(L^{DNP})_{24}(ring)_7(PF_6)_{44}$]	8^+	3154.3671	3154.4157
[$Pd_{12}(L^{DNP})_{24}(ring)_7(PF_6)_{43}$]	9^+	2787.8850	2787.9291
[$Pd_{12}(L^{DNP})_{24}(ring)_8(PF_6)_{48}$]	8^+	3292.0064	3292.0559
[$Pd_{12}(L^{DNP})_{24}(ring)_8(PF_6)_{47}$]	9^+	2910.1189	2910.1647
[$Pd_{12}(L^{DNP})_{24}(ring)_9(PF_6)_{51}$]	9^+	3032.3528	3032.4003

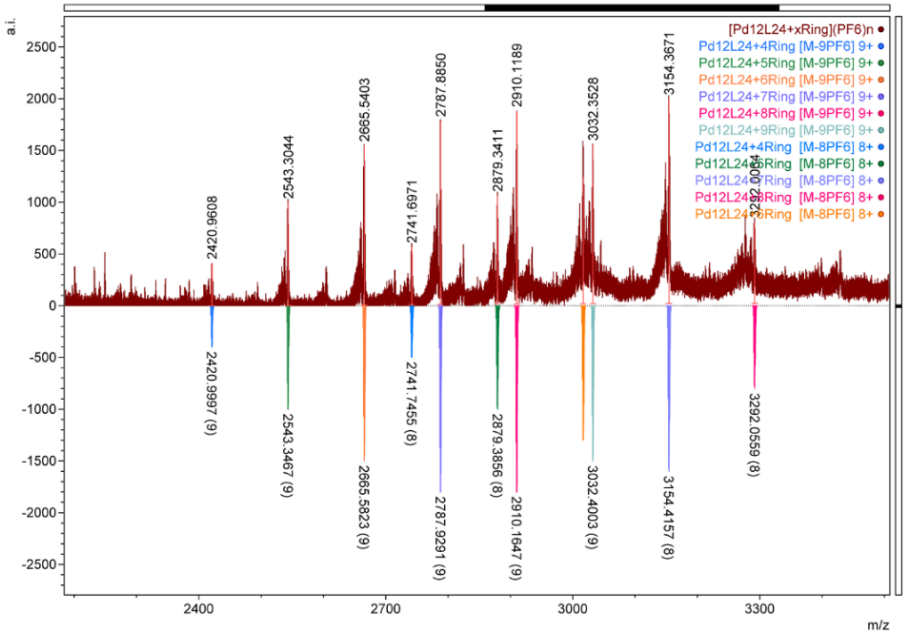

Figure 25. Full ESI–MS signals for nanosphere sample $\mathbf{[Pd_{12}(L^{DNP})_{24}(ring)_m(PF_6)_{24}]}$.

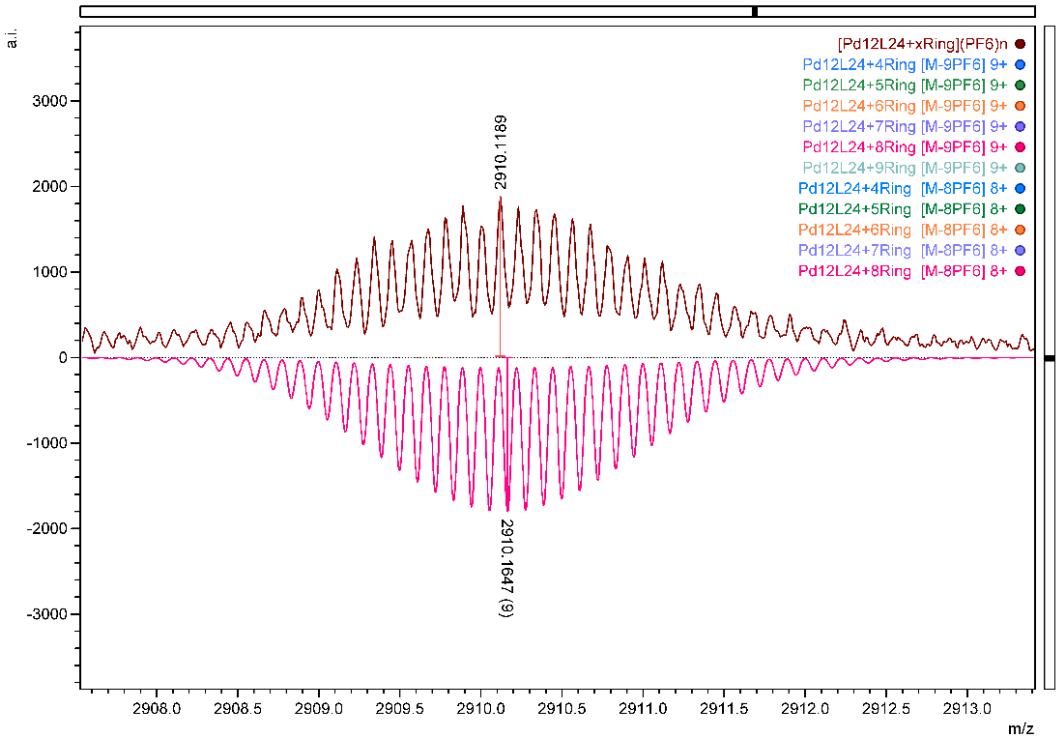

Figure 26. ESI–MS signal for $\mathbf{[Pd_{12}(L^{DNP})_{24}(ring)_8(PF_6)_{47}]^{9+}}$, *m/z* = 2910.1189, calculated *m/z* = 2910.1647.

S6.4. Determination of ring binding to nanosphere sample [$Pd_{12}(L^{DNP})_{24}(ring)_m$ $(PF_6)_{24}$]

To determine average amount of **ring** binding the distribution represented in Supplementary Figure 27 was fitted with *Origin 9.0 (Academic)* using the Gaussian function (Equation 2.)

$$y = y_0 + \frac{A}{w\sqrt{\pi/2}} \times e^{-\frac{(x-x_c)^2}{2w^2}} \qquad (2)$$

In Equation 2, A represents area under the peak, w is two times σ (standard deviation) and x_c is the center of the peak. The value for y_0 is the baseline offset and was fixed at 0. For fitting results for sample coefficient of determination (R^2) was found ($R^2 = 0.9792$). Binding of **ring** was determined $x_c = 8$ and $\sigma = 2.238$. This implies that 95% of the nanospheres in this sample bind 8 ± 5 **ring** molecules.

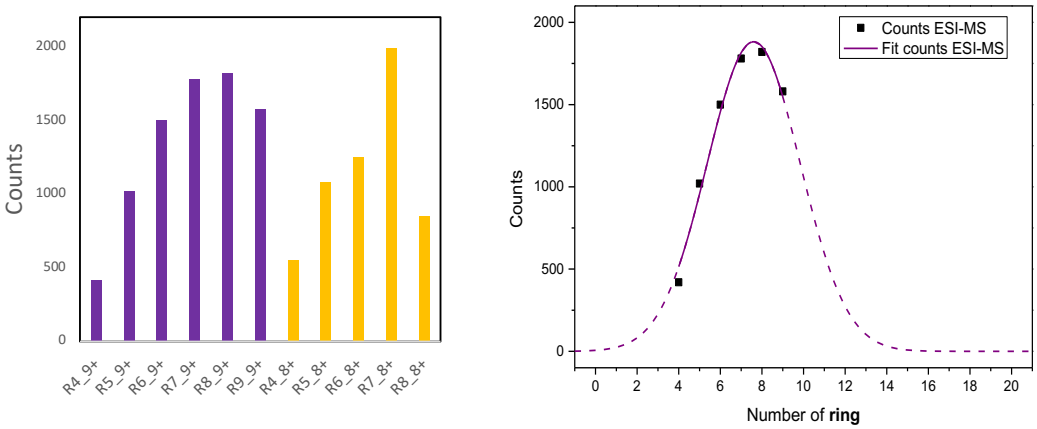

Figure 27. Distribution of **ring**s amongst 9^+ species and 8^+ species for nanosphere sample **[$Pd_{12}(L^{DNP})_{24}(ring)_m(PF_6)_{24}$]**. (left) and normal distribution of **ring** amongst 9^+ species based on ESI–MS (Supplementary Figure 25). The data was fitted with a Gaussian function using *Origin 9.0* (Equation 2).

S7. Kinetic insight through ESI–MS

Nanosphere formation via Pathway 1 (with **ring**) at 25°C

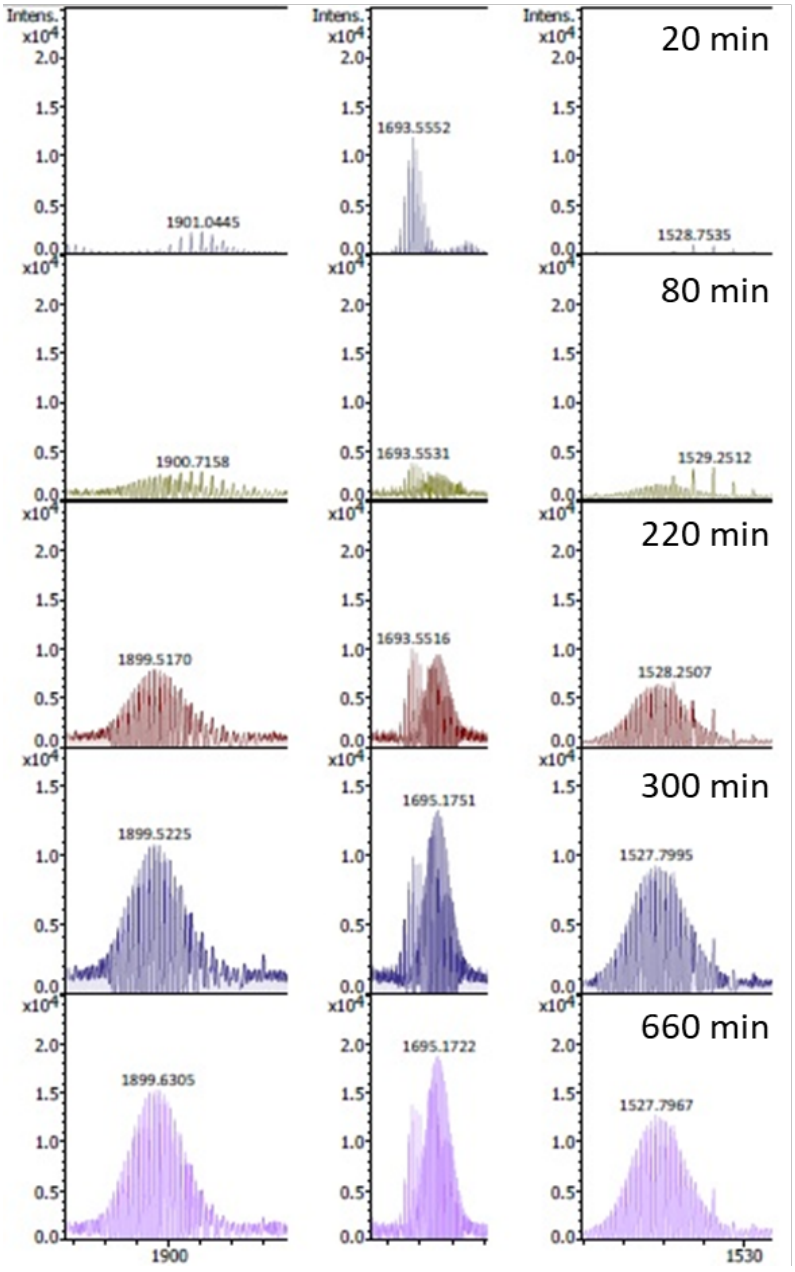

Figure 28. ESI–MS peak for $[Pd_{12}(L^{DNP})_{24}(ring)_m(BF_4)_n(PF_6)_{24-n}]^{9-11+}$, recorded at (from top to bottom) 20, 80, 220, 300 and 660 min. The final intensity for all nanosphere peaks at *m/z* = 1680 was set at 100% and all other intensities found over time were normalized to this value.

Nanosphere formation via Pathway 2 (no **ring**) at 25°C

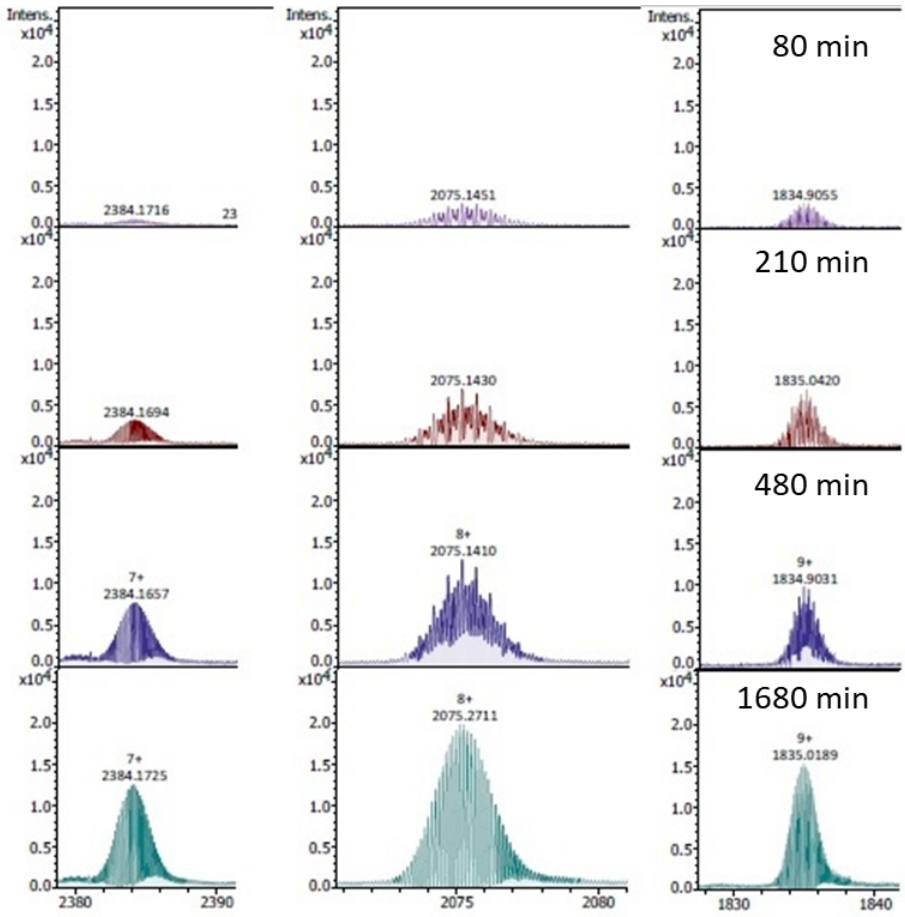

Figure 29. ESI–MS peak for $\mathbf{[Pd_{12}(L^{DNP})_{24}](BF_4)_n^{7-9+}}$, recorded at (from top to bottom) 20, 80, 210, 480 and 1680 min. The final intensity for all nanosphere peaks at *m/z* = 1680 was set at 100% and all other intensities found overtime were normalized to this value.

S8. Molecular dynamic simulations

Method description for molecular dynamics simulations

Model structures of Pd_nL_m assembly intermediates (**L** = $\mathbf{L^{MeO}}$, $\mathbf{L^{DNP}}$ or $\mathbf{L^{DNP}}$ + **ring**) were constructed using a previously described template approach with 1–12 palladium centers.[15] Then, using the Amber16 software suite,[16] these initial structures were minimized and propagated with implicit solvent molecular dynamics to produce 100 ns trajectories. The resulting trajectory data were then processed using *cpptraj* to compute RMSD, pucker,[17] and molecular strain (Equation 3).[16]

$$E = \frac{E_{amber}(\mathrm{Pd}_n\mathbf{L}_\mathrm{m}) - n \times E_{amber}(\mathrm{Pd}) - m \times E_{amber}(\mathbf{L})}{n} \quad (3)$$

Equation 3. The relative configuration energy of a nanosphere intermediate is computed as the difference between the Amber forcefield energy (E_{amber}) of the intermediate assembly (Pd_nL_m) and the sum of the forcefield energy of its constituent parts Pd and **L** (**L** = $\mathbf{L^{MeO}}$, $\mathbf{L^{DNP}}$ or $\mathbf{L^{DNP}}$ + **ring**), scaled by the total number of metal centers (n).

Structural dynamics of penta-nuclear intermediates

Simulated structures of intermediates were produced using a template of the complete $Pd_{12}L_{24}$ sphere (**L** = $\mathbf{L^{MeO}}$, $\mathbf{L^{DNP}}$ or $\mathbf{L^{DNP}}$⊂**ring**). We observed that over the course of dynamics simulations that intermediate assemblies may convert from their initial spherical shape to a flat conformation. This is readily shown with pentanuclear intermediates Pd_5L_{14} (**L** = $\mathbf{L^{MeO}}$, $\mathbf{L^{DNP}}$ or $\mathbf{L^{DNP}}$ + **ring**), using the palladium atom RMSD and ring pucker parameter devised by Cremer and Pople.

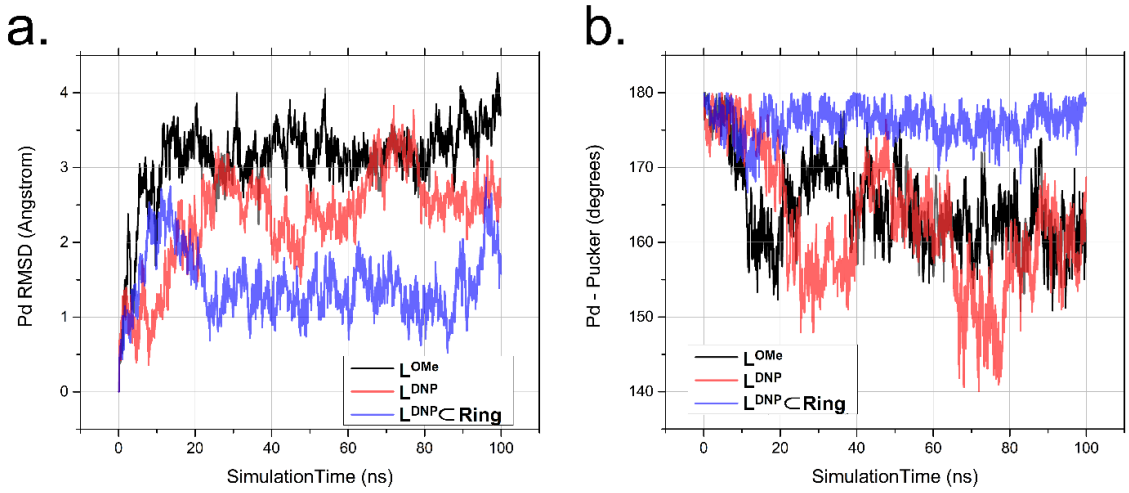

Figure 30. a) Geometric descriptors, RMSD and b) Cremer's ring pucker[17] of trajectories for $Pd_5(\mathbf{L^{OMe}})_{14}$ (black), $Pd_5(\mathbf{L^{DNP}})_{14}$ (red), and $Pd_5(\mathbf{L^{DNP}\subset ring})_{14}$ (blue).

The flexibility of the intermediate assembly allows for the arrangement of palladium atoms to move away from the 'ideal' configuration of the $Pd_{12}L_{24}$ nanosphere. We observe that intermediates constructed with $\mathbf{L^{OMe}}$ or $\mathbf{L^{DNP}}$ undergo more significant conformational changes leading to a greater RMSD value (Supplementary Figure 30a) than those constructed with $\mathbf{L^{DNP}\subset ring}$. The significance of this change is evidenced by comparing the 'pucker' parameter of the palladium centers that shows a significant shift away from 180° (i.e., near spherical) pucker found for the nanosphere structure towards flatter configurations (i.e., 140–170°). From these results we surmise that the ring hinders this conformational change and promotes curvature of the forming intermediate. Decomposition of non-bonded energies (data not shown) further indicate that this barrier arises from electrostatic force field terms (i.e., charge-repulsion) rather than steric effects.

These MD results provide further detail into the self-assembly pathway enabled by the ring effect. The increase in curvature of the intermediate species leads to the formation of a spherical structure of finite size (i.e., a nanosphere), thereby preventing indefinite polymeric assemblies.

This is further illustrated by the structures produced from 100 ns MD simulations (Supplementary Figure 31).

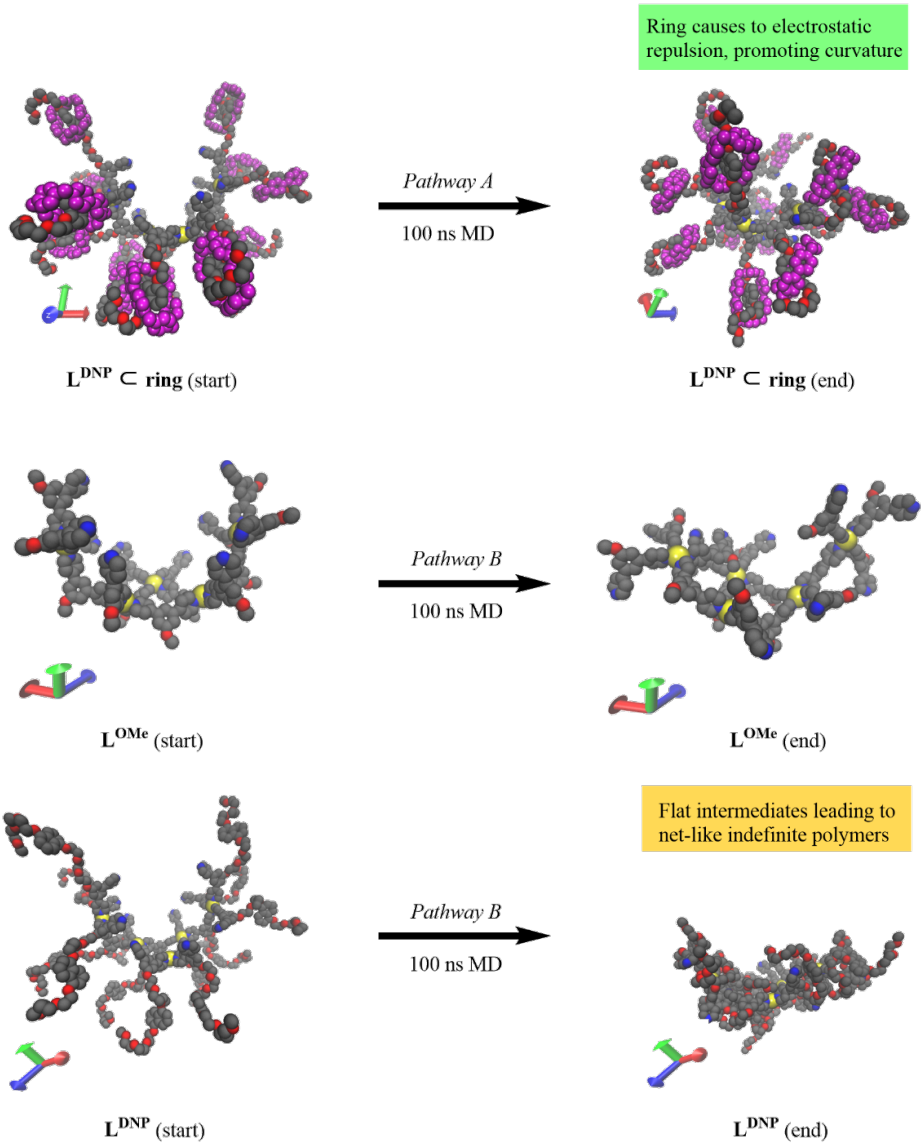

Figure 31. Visualization of the MD trajectory propagated for $Pd_5(\mathbf{L^{DNP}\subset ring})_{14}$, $Pd_5(\mathbf{L^{OMe}})_{14}$ and $Pd_5(\mathbf{L^{DNP}})_{14}$ as snapshots after 0 ns (start) and 100 ns (end).

Influence of strain on nanosphere formation

We quantified the thermodynamic effects of ring association by comparing the configurational energy (Equation 3) of intermediate species for Pd_nL_m assemblies (n =1–12, m = 2n–3n, L = $\mathbf{L^{MeO}}$, $\mathbf{L^{DNP}}$ or $\mathbf{L^{DNP}}$ + **ring**) as a function of assembly size (Supplementary Figure 32). These results show that nanosphere formation must overcome a thermodynamic barrier arising with the formation of a penta-nuclear intermediate (Supplementary Figure 32, n = 5). From the changes in curvature (i.e., pucker, Supplementary Figure 30b) and visual analysis (Supplementary Figure 31), we surmise that this unfavorable peak arises from the observed conformational changes of the intermediate assembly. As the association of ring to $\mathbf{L^{DNP}}$ limits these conformational changes (see Supplementary Figure 30a & S31), we observe a decrease in the barrier for the formation of the final nanosphere structure.

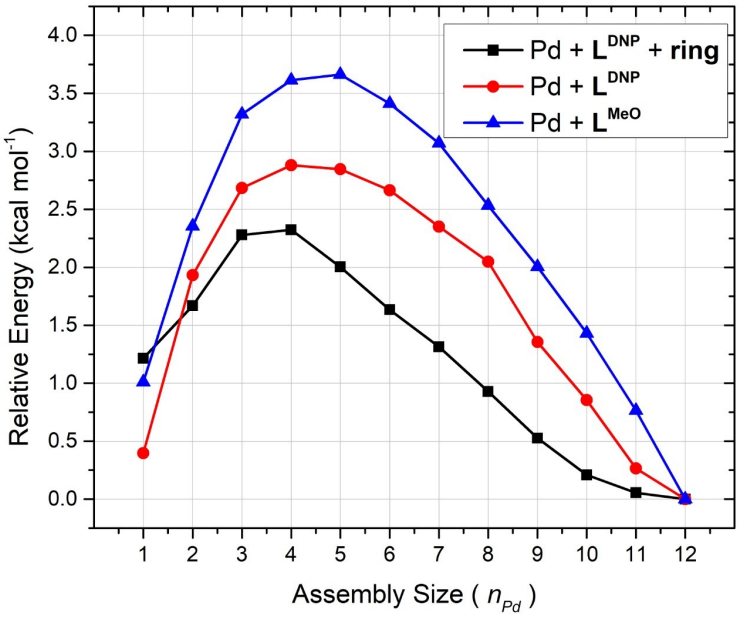

Figure 32. The relative energy of model intermediate assemblies for the formation of cuboctahedral $Pd_{12}L_{24}$ nanospheres (L = $\mathbf{L^{MeO}}$, $\mathbf{L^{DNP}}$ or $\mathbf{L^{DNP}}$ + **ring**). Energies were computed based on the per Pd energy differences arising from the coordination bond network (Equation S3) relative to the complete $Pd_{12}L_{24}$ nanosphere. Nanospheres featuring bound ring were constructed assuming 1:1 binding of $\mathbf{L^{DNP}}$ and ring using a pre-bound [$\mathbf{L^{DNP}}$ + **ring**] ligand model.

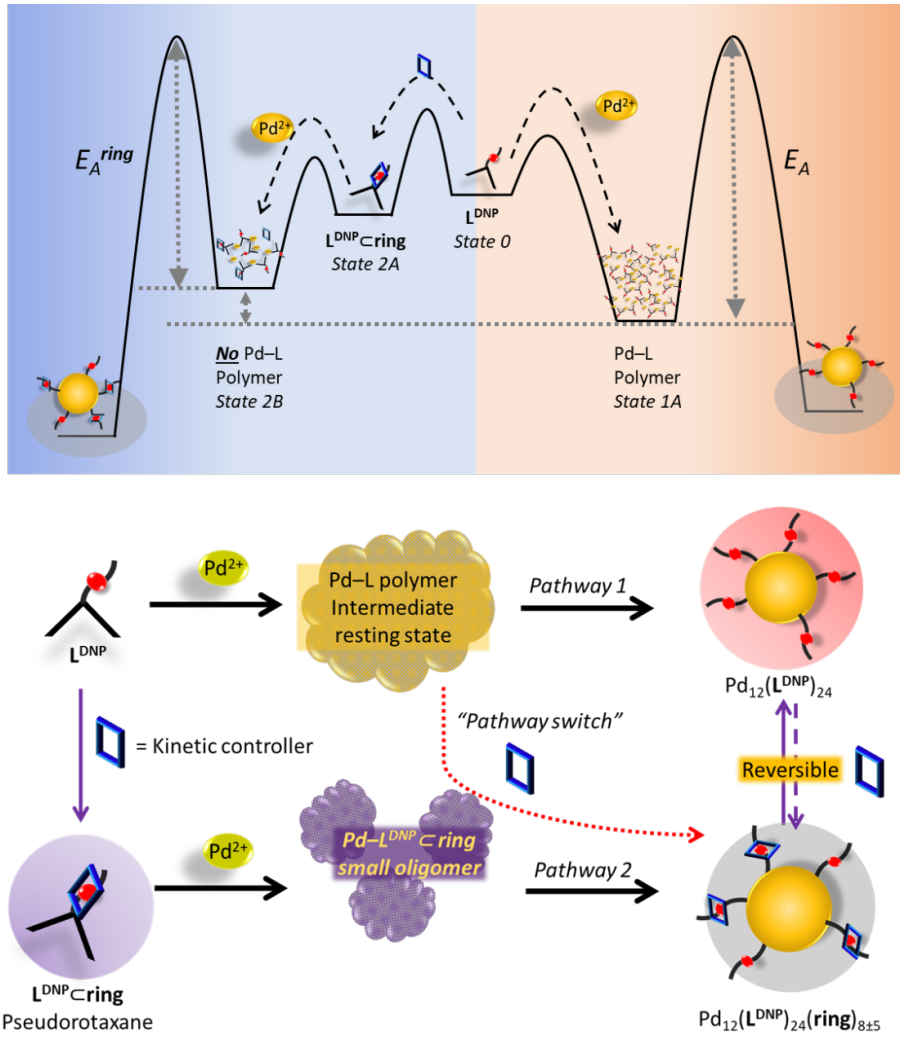

Figure 33. Proposed energy landscape based on kinetic studies. $\mathbf{L^{DNP}}$ nanosphere formation occurs via the Pd–L polymer intermediate (Pathway 1, right, orange). The Pd–L polymer is a low energy resting state which becomes a kinetically trapped species at low temperature. In presence of ring (Pathway 2, left, blue), this Pd–L polymer intermediate is destabilized, increasing the energy of the resting state. Accordingly, the activation barrier E_A^{ring} is lower than E_A in absence of ring

S9. References

1. Bouwens, T., Mathew, S. & Reek, J. N. H. p-Type dye-sensitized solar cells based on pseudorotaxane mediated charge-transfer. *Faraday Discuss* **215**, 393–406 (2019).
2. Jiang, F. *et al.* Thiophene-Coated Functionalized M 12 L 24 Spheres: Synthesis, Characterization, and Electrochemical Properties. *Chem Asian J* **7**, 2230–2234 (2012).
3. Wang, X. *et al.* Tuning the Porphyrin Building Block in Self-Assembled Cages for Branched-Selective Hydroformylation of Propene. *Chem. Eur. J.* **23**, 14769–14777 (2017).
4. Wang, A., Huang, J. & Yan, Y. Hierarchical molecular self-assemblies: construction and advantages. *Soft Matter* **10**, 3362–3373 (2014).
5. Viljoen, E., Zhu, K. & Loeb, S. J. From Binuclear Complexes to Molecular Necklaces: Incorporating Flexible Ligands into Rotaxanes. *Chemistry - A European Journal* **22**, 7479–7484 (2016).
6. Datta, S., Saha, M. L. & Stang, P. J. Hierarchical Assemblies of Supramolecular Coordination Complexes. *Acc Chem Res* **51**, 2047–2063 (2018).
7. Ferrando-Soria, J. *et al.* A [13]rotaxane assembled via a palladium molecular capsule. *Nat Commun* **10**, 3720 (2019).
8. Hunter, C. A. & Anderson, H. L. What is cooperativity? *Angew. Chem. Int. Ed.* **48**, 7488–7499 (2009).
9. Gramage-Doria, R. *et al.* Gold(I) Catalysis at Extreme Concentrations Inside Self-Assembled Nanospheres. *Angewandte Chemie International Edition* **53**, 13380–13384 (2014).
10. Sun, Q.-F., Sato, S. & Fujita, M. An M 12 (L 1) 12 (L 2) 12 Cantellated Tetrahedron: A Case Study on Mixed-Ligand Self-Assembly. *Angewandte Chemie International Edition* **53**, 13510–13513 (2014).
11. Venturi, M., Dumas, S., Balzani, V., Cao, J. & Stoddart, J. F. Threading/dethreading processes in pseudorotaxanes. A thermodynamic and kinetic study. *New Journal of Chemistry* **28**, 1032–1037 (2004).
12. Castro, R., Nixon, K. R., Evanseck, J. D. & Kaifer, A. E. Effects of Side Arm Length and Structure of *Para* -Substituted Phenyl Derivatives on Their Binding to the Host Cyclobis(paraquat- *p* -phenylene). *J Org Chem* **61**, 7298–7303 (1996).
13. Fahrenbach, A. C., Bruns, C. J., Cao, D. & Stoddart, J. F. Ground-State Thermodynamics of Bistable Redox-Active Donor–Acceptor Mechanically Interlocked Molecules. *Acc Chem Res* **45**, 1581–1592 (2012).
14. Bruns, C. J. *et al.* Emergent Ion-Gated Binding of Cationic Host–Guest Complexes within Cationic M 12 L 24 Molecular Flasks. *J Am Chem Soc* **136**, 12027–12034 (2014).
15. Poole, D. A., Bobylev, E. O., Mathew, S. & Reek, J. N. H. Topological prediction of palladium coordination cages. *Chem Sci* **11**, 12350–12357 (2020).
16. Götz, A. W. *et al.* Routine Microsecond Molecular Dynamics Simulations with AMBER on GPUs. 1. Generalized Born. *J Chem Theory Comput* **8**, 1542–1555 (2012).
17. Cremer, D. & Pople, J. A. General definition of ring puckering coordinates. *J Am Chem Soc* **97**, 1354–1358 (1975).